JBC RESEARCH ARTICLE

Binding with heat shock cognate protein HSC70 fine-tunes the Golgi association of the small GTPase ARL5B

Received for publication, September 15, 2021, and in revised form, November 4, 2021 Published, Papers in Press, November 16, 2021,
https://doi.org/10.1016/j.jbc.2021.101422

Ebsy Jaimon, Aashutosh Tripathi, Arohi Khurana, Dipanjana Ghosh, Jini Sugatha, and Sunando Datta*
From the Department of Biological Sciences, Indian Institute of Science Education and Research Bhopal, Bhopal, India

Edited by Ursula Jakob

ARL5B, an ARF-like small GTPase localized to the trans-Golgi, is known for regulating endosome-Golgi trafficking and promoting the migration and invasion of breast cancer cells. Although a few interacting partners have been identified, the mechanism of the shuttling of ARL5B between the Golgi membrane and the cytosol is still obscure. Here, using GFP-binding protein (GBP) pull-down followed by mass spectrometry, we identified heat shock cognate protein (HSC70) as an additional interacting partner of ARL5B. Our pull-down and isothermal titration calorimetry (ITC)-based studies suggested that HSC70 binds to ARL5B in an ADP-dependent manner. Additionally, we showed that the N-terminal helix and the nucleotide status of ARL5B contribute to its recognition by HSC70. The confocal microscopy and cell fractionation studies in MDA-MB-231 breast cancer cells revealed that the depletion of HSC70 reduces the localization of ARL5B to the Golgi. Using *in vitro* reconstitution approach, we provide evidence that HSC70 fine-tunes the association of ARL5B with Golgi membrane. Finally, we demonstrated that the interaction between ARL5B and HSC70 is important for the localization of cation independent mannose-6-phosphate receptor (CIMPR) at Golgi. Collectively, we propose a mechanism by which HSC70, a constitutively expressed chaperone, modulates the Golgi association of ARL5B, which in turn has implications for the Golgi-associated functions of this GTPase.

ARF-like proteins (ARLs) belong to the ARF family of small GTPases and perform diverse functions such as membrane trafficking, tubulin assembly, lysosome positioning, etc. (1–3). Being small GTPases, they alternate between a GDP-bound and a GTP-bound form, and the nucleotide cycling is coupled to their association with the membrane, where they perform their downstream functions (4, 5). For ARFs and ARLs, an extended N-terminal amphipathic helix is often myristoylated and further facilitates their membrane attachment (6, 7).

The GDP/GTP cycle of GTPases is regulated by Guanine nucleotide Exchange Factors (GEFs), which exchange the bound GDP with GTP and GTPase-Activating Proteins (GAPs) that accelerate the GTPase rate. Many of these factors have been identified for ARFs, but only a few of them are known for ARLs. A group of proteins called GDP-dissociation inhibitors (GDIs) are known to help Rab and Rho GTPases cycle between membrane and cytosol (8, 9). In addition, there are GDI-like factors, including the chaperones SmgGDS and PDEdelta, which can deliver as well as extract small GTPases (Ras and Rap) to and from the membrane (10, 11). To date, no GDIs or GDI-like factors have been reported for ARFs and ARLs (12).

ARF-like 5B (ARL5B), a predominantly Golgi-localized member of the ARL subfamily, regulates the retrograde and anterograde trafficking of cargoes between Golgi and endosomes through effectors such as GARP (a tethering factor) and AP-4 (an adaptor protein complex), respectively (13–15). Moreover, a recent study has also implicated its role in promoting migration and invasion in breast cancer cell lines (16). To date, only a few regulators are known for ARL5B. ARFRP1, an ARL, coordinates GARP recruitment, perhaps by recruiting a GEF for ARL5 (17). Ragulator functions as a GEF for ARL5B at endolysosome and regulates trafficking of proteins from endosomes to Golgi in response to the stimulation by amino acids (18). However, the mechanism by which ARL5B cycles between Golgi and cytosol is largely elusive.

Heat Shock Cognate Protein 70 (HSC70) is a constitutively expressed member of the HSP70 family of chaperones. HSC70 consists of an N-terminal Nucleotide-Binding Domain (NBD), a linker, a Substrate-binding Domain (SBD), and an unstructured C-terminal tail. The conformational changes due to ADP/ATP cycling at the NBD allosterically regulate the binding of a diverse set of substrates at the SBD and thereby enable the chaperone to carry out various cellular functions such as disassembly/assembly of coat proteins, protein translocation across membranes, chaperone-mediated autophagy, and microautophagy (19–22).

For most of the small GTPases, spatiotemporal regulation of their membrane localization greatly impacts their function. Therefore, dissecting the mechanism of cycling of any small GTPase between membrane and cytosol is of utmost importance to understand their functioning at a greater depth. In this study, we identify HSC70 as an interacting partner of ARL5B and investigate its novel role in the Golgi localization of ARL5B. Further, we explore the implication of HSC70-ARL5B interaction in the intracellular distribution of CIMPR.

* For correspondence: Sunando Datta, sunando@iiserb.ac.in.

© 2021 THE AUTHORS. Published by Elsevier Inc on behalf of American Society for Biochemistry and Molecular Biology. This is an open access article under the CC BY license (http://creativecommons.org/licenses/by/4.0/).

Results

HSC70 interacts with ARL5B in an ADP-dependent manner

To identify the interacting partners of ARL5B, we employed a nanobody-based GFP-binding protein (GBP) pull-down assay (23, 24). We expressed ARL5B-GFP protein in MDA-MB-231 cells using the Lenti-X Tet-On 3G inducible expression system (Fig. S1*A*). GST-tagged GBP (Fig. S1*B*) was immobilized on glutathione sepharose beads and incubated with lysate extracted from cells expressing ARL5B-GFP or GFP. The pulled-down proteins were eluted, separated on SDS-PAGE, and analyzed by silver staining. We detected a band <75 kD specific to the eluate lane of ARL5B-GFP and absent in the lane of GFP (Fig. 1*A*). The band was excised, digested with trypsin, and subjected to mass spectrometry (MALDI-TOF). Using peptide mass fingerprinting (PMF), we identified the protein as HSC70 (HSP7C) with an expect value <0.05 (Table S1, raw data deposited at https://doi.org/10.6084/m9.figshare.16429140.v2). We validated the mass spectrometry result by performing the GBP pull-down assay and analyzing the eluates by immunoblotting using an anti-HSC70 antibody. The pull-down result confirmed that HSC70 is bound specifically with ARL5B-GFP and not GFP (Fig. 1*B*). Next, to determine whether HSC70 directly interacts with ARL5B, we purified recombinant GST-HSC70 and His-ARL5B (Fig. S1*C*). As revealed by the HPLC analysis, the purified His-ARL5B was 84% GDP-bound (Fig. S1*D*). We immobilized His-ARL5B on Ni-NTA agarose beads and incubated it with GST-HSC70. The unbound protein was removed by washes, and the eluates were subjected to SDS-PAGE followed by immunoblotting using an anti-HSC70 antibody. The result from the binding assay showed that HSC70 interacts directly with ARL5B (Fig. 1*C*).

HSC70 belongs to the HSP70 family of chaperones and is known to bind to a range of substrates with high affinity when bound to ADP and low affinity when bound to ATP (25). We next tested whether HSC70 binds to ARL5B in a nucleotide-dependent manner. We performed a His pull-down assay where His-ARL5B protein was immobilized on Ni-NTA beads and incubated with MDA-MB-231 cell extracts in the presence of 5 mM ADP or 5 mM ATP. The eluates were resolved through SDS-PAGE and subjected to immunoblotting using an anti-HSC70 antibody. We found that ARL5B pulled down HSC70 specifically in the presence of ADP compared with ATP (Fig. 1*D*). We also carried out a His pull-down-based binding assay by incubating purified His-ARL5B with GST-HSC70 in the presence of 5 mM ADP or 5 mM ATP. Following washes, we analyzed the proteins by immunoblotting. The result from the binding assay showed that ARL5B interacted with HSC70 preferentially in the presence of ADP compared with ATP (Fig. 1*E*). Next, we performed isothermal titration calorimetry (ITC) to determine the affinity of the interaction between ARL5B and HSC70. In this assay, we titrated 1 μM of His-HSC70 with 30 μM of His-ARL5B in the presence of 5 mM of ADP or 5 mM ATP. The ITC results revealed that HSC70 binds to ARL5B with an association constant (Ka) of 9.44×10^7 M^{-1} in the presence of ADP, and the interaction is enthalpy driven. In contrast, we found no interaction in the presence of ATP (Figs. 1*F* and S1*E*). We obtained the thermodynamic parameters after fitting the raw data into a 1:1 binding model as shown in Figure 1*G*. Collectively, our results suggest that HSC70 interacts with ARL5B in an ADP-dependent manner.

Recognition by HSC70 is determined by the N-terminal helix and the nucleotide status of ARL5B

Previous studies have shown that the proteins of the HSP70 family recognize hydrophobic and basic residues (26, 27). The presence of such residues in the N terminal helix of ARL5B prompted us to check whether HSC70 recognizes the N-terminal helix for the binding. To delineate the importance of the N-terminal helix of ARL5B in binding to HSC70, we deleted the first 15 residues from the N-terminal of ARL5B, denoted as [ΔN15]ARL5B, and purified the His-tagged [ΔN15]ARL5B protein (Fig. S2*A*). We did a His pull-down assay by immobilizing His-ARL5B and His-[ΔN15]ARL5B on Ni-NTA beads and incubating with MDA-MB-231 cell extracts. Immunoblotting using an anti-HSC70 antibody showed that although HSC70 interacted with full-length ARL5B, almost no binding was detected with [ΔN15]ARL5B (Fig. 2*A*). Besides MDA-MB-231, we validated the result in HeLa cells. His-ARL5B pulled down HSC70 from HeLa cell lysate, whereas His-[ΔN15]ARL5B did not (Fig. 2*B*). We further confirmed this observation by performing a His pull-down-based binding assay where we incubated GST-HSC70 with His-ARL5B and His-[ΔN15]ARL5B immobilized on Ni-NTA beads. HSC70 bound preferentially with full-length ARL5B, and minimal binding was seen with [ΔN15]ARL5B (Figs. 2*C* and S2*B*). The importance of the N-terminal residues was also evaluated by ITC, where 1 μM of His-HSC70 protein was titrated with 30 μM of His-[ΔN15]ARL5B in the presence of 5 mM of ADP. The ITC result confirmed that His-[ΔN15]ARL5B does not bind to HSC70 (Fig. 2*D*).

The GFP-tagged [ΔN15]ARL5B localizes in the cytoplasm and the nucleus and was completely absent from Golgi, signifying the importance of the N-terminal helix in the Golgi association (Fig. S2*C*). We also performed CD spectroscopy to verify whether the deletion of the N-terminal residues perturbed the overall secondary structure of ARL5B and consequently affected the binding with HSC70. The far-UV CD spectra analysis indicated no gross change in the secondary structure of His-[ΔN15]ARL5B compared with His-ARL5B (Fig. S2*D*). Further, in an attempt to identify the residues important for recognition by HSC70, we first mutated a few hydrophobic residues (L8A, F12A, L8AF12A) and a basic residue (K7E) in the N-terminal of ARL5B. His pull-down assay revealed that these mutations did not abrogate the interaction with HSC70 (Fig. S2, *E*–*G*). HSC70 is also known to recognize KFERQ-like motifs and target proteins for degradation through chaperone-mediated autophagy (28). We identified a potential KFERQ-like sequence ($_{15}$QEHKV$_{19}$) in the N terminus of ARL5B. Since it was known that mutating Q alone in the KFERQ-like sequence was sufficient to perturb the

ASBMB

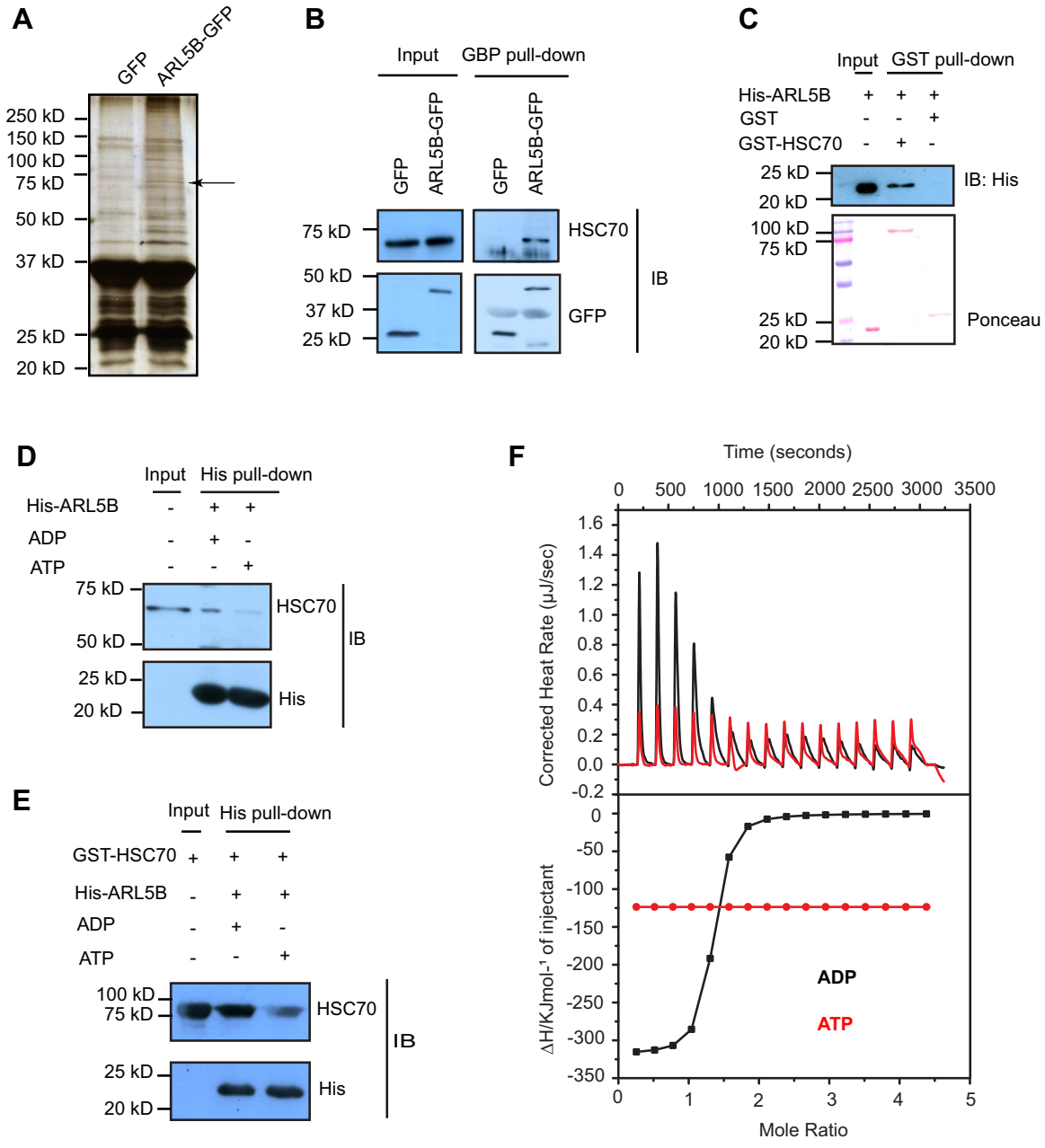

G

ARL5B (µM)	HSC70 (µM)	ΔH (kJmol-1)	ΔS (Jmol-1K-1)	TΔS (kJmol-1)	ΔG (kJmol-1)	Ka (M-1)	n
30	1	-318.7	-916.2	-273.02	-45.68	$9.44x10^7$	1.24

Figure 1. HSC70 binds to ARL5B in an ADP-dependent manner. *A*, 1 mg of the lysate of MDA-MB-231 cells expressing GFP or ARL5B-GFP was incubated with 25 µg of GST-GBP immobilized on glutathione sepharose beads. The pull-down was analyzed by silver staining. The *arrow points* toward the band that was excised and identified by mass spectrometry. *B*, the pull-down was performed as in (*A*) and analyzed by immunoblotting using anti-GFP and anti-HSC70 antibodies. *C*, bacterially expressed and purified GST or GST-HSC70 (0.06 µM) immobilized on glutathione sepharose beads was incubated with purified His-ARL5B (0.25 µM), and the binding was detected by immunoblotting using an anti-His antibody. Ponceau staining shows the bait proteins. *D*, 25 µg of His-ARL5B immobilized on Ni-NTA beads was incubated with 400 µg of MDA-MB-231 lysate in the presence of 5 mM ADP or 5 mM ATP. The pull-down was subjected to immunoblotting using anti-His and anti-HSC70 antibodies. *E*, bacterially expressed and purified His-ARL5B (0.25 µM) was incubated with purified GST-HSC70 (0.06 µM) in the presence of 5 mM ADP or 5 mM ATP. The binding was detected by immunoblotting using anti-HSC70 and anti-His antibodies. *F*, the raw ITC data (*top*) and integrated normalized data (*bottom*) for the titration of 30 µM of His-ARL5B with 1 µM of His-HSC70 in the presence of 5 mM ADP (*black*) and 5 mM ATP (*red*). *G*, table shows the thermodynamic parameters obtained for the measured interaction.

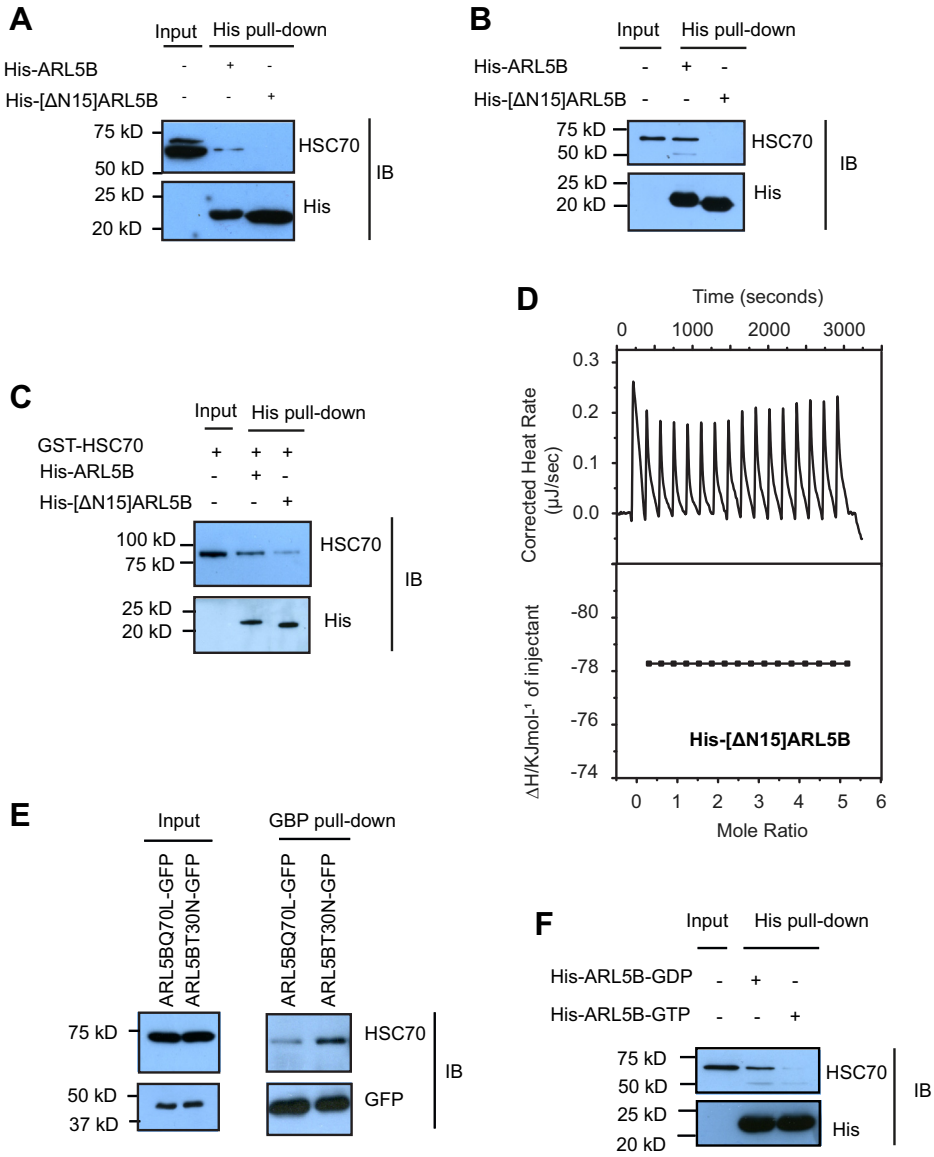

Figure 2. N-terminal helix and nucleotide status of ARL5B determines recognition by HSC70. *A*, 25 μg of His-ARL5B or His[ΔN15]ARL5B immobilized on Ni-NTA beads was incubated with 400 μg of MDA-MB-231 lysate, and the pull-down was analyzed using anti-HSC70 and anti-His antibodies. *B*, 25 μg of His-ARL5B or His-[ΔN15]ARL5B immobilized on Ni-NTA agarose beads was incubated with 400 μg of HeLa cell lysate, and the pull-down was analyzed by immunoblotting using anti-His and anti-HSC70 antibodies. *C*, 0.25 μM of purified His-ARL5B or His-[ΔN15]ARL5B was incubated with 0.06 μM of purified GST-HSC70, and the binding was detected by immunoblotting using anti-HSC70 and anti-His antibodies. *D*, the raw ITC data (*top*) and integrated normalized data (*bottom*) for the titration of 30 μM of His-[ΔN15]ARL5B with 1 μM of His-HSC70 in the presence of 5 mM ADP. *E*, 500 μg lysate of HeLa cells expressing ARL5BQ70L-GFP or ARL5BT30N-GFP was incubated with 25 μg GST-GBP bound to glutathione sepharose beads in the presence of 5 mM of GTP and 5 mM of GDP, respectively. The pull-down was analyzed by immunoblotting using anti-GFP and anti-HSC70 antibodies. The quantification of the immunoblot by densitometric analysis from three independent experiments is shown in Figure S3*B*. *F*, 25 μg of His-ARL5B-GDP or His-ARL5B-GTP immobilized on Ni-NTA beads was incubated with 400 μg of MDA-MB-231 lysate. GDP or GTP was added 50-fold more than the concentration of His-ARL5B-GDP or His-ARL5B-GTP, respectively. The pull-down was subjected to immunoblotting using anti-His and anti-HSC70 antibodies.

interaction with HSC70 (29) and the [ΔN15]ARL5B, which could not interact with HSC70 was devoid of Q at the 15th position, we also mutated the KFERQ-like motif in ARL5B (Q15A, Q15AE16A, Q15AK18A) and performed His pull-down assay. Our results indicated that none of these mutations abolished the interaction with HSC70 (Fig. S2, *H–J*).

We next investigated whether the recognition by HSC70 depends on the nucleotide status of ARL5B. We utilized constitutively active (ARL5Q70L) and dominant negative (ARL5BT30N) mutants of ARL5B, which is GTP restricted and GDP restricted, respectively. We performed a GBP pull-down assay using the lysate extracted from HeLa cells expressing GFP-tagged ARL5BQ70L and ARL5BT30N mutants of ARL5B. The pull-down result showed that HSC70 bound relatively more with ARL5BT30N, the GDP restricted and dominant negative mutant of ARL5B (Figs. 2*E* and S3, *A* and *B*). This result was further confirmed by carrying out a His pull-down assay where GDP or GTP loaded His-ARL5B immobilized on Ni-NTA agarose beads was incubated with MDA-MB-231 cell lysate. The GDP-loaded ARL5B was 96% GDP-bound, and the GTP-loaded ARL5B was 70% GTP-bound and 30% GDP-bound, as evident from the HPLC

analysis (Fig. S3*C*). The pull-down result revealed that HSC70 is preferentially bound with ARL5B-GDP from MDA-MB-231 lysate (Fig. 2*F*). However, when we incubated bacterially expressed and purified GST-HSC70 with His-ARL5B-GDP or His-ARL5B-GTP, we noted that HSC70 bound equally with ARL5B-GDP and ARL5B-GTP (Fig. S3*D*). We confirmed this result by ITC, where we titrated 1 μM of His-HSC70 with 30 μM of His-ARL5B-GDP or His-ARL5B-GTP in the presence of 5 mM of ADP (Fig. S3, *E*–*F*). Taken together, our results suggest that the N-terminal helix and the nucleotide status of ARL5B contribute to the recognition by HSC70.

Depletion of HSC70 reduces the Golgi localization of ARL5B

Since the N-terminal helix in the ARF family of GTPases is important for their membrane association (5) and the recognition of ARL5B by HSC70 is mediated by the N-terminal helix, it pointed toward a possibility that HSC70 could play a role in the membrane-associated function of ARL5B. To investigate the functional relevance of the HSC70-ARL5B interaction, we used three independent siRNA oligos targeting HSC70. We confirmed the knockdown efficiency of siRNA oligos at the mRNA (Fig. S4*A*) and protein level (Fig. S4*B*). Next, we checked the localization of ARL5B in MDA-MB-231 cells by treating them with individual HSC70 siRNA oligos. The cells were fixed, immunostained for endogenous ARL5B and Golgi markers such as Giantin (17) and Golgin-97 (30), and images were acquired by a laser scanning confocal microscope (Fig. S4, *C* and *D*). As evident from the object-based colocalization calculated using Motion tracking (31, 32), the colocalization of ARL5B with Giantin and Golgin-97 was significantly reduced in cells treated with HSC70 siRNA oligos (Fig. S4, *E* and *F*). To further support our results, we assessed the membrane-associated levels of ARL5B by performing a cell fractionation experiment. We observed that ARL5B in the membrane fraction is 66% reduced in the cells treated with HSC70 siRNA (Fig. S4, *G* and *H*). As the total level of ARL5B was 57% reduced in HSC70 knockdown cells (Fig. S4, *I* and *J*), there exists a possibility that the reduction in ARL5B levels consequently affected the membrane-bound levels of ARL5B. Therefore, we normalized ARL5B in the membrane-bound fraction with respect to the total level of ARL5B and found that the ARL5B associated with the membrane is 20% reduced in HSC70 knockdown cells compared with the control cells.

To rule out the off-target effects, we further generated the HSC70 knockout MDA-MB-231 cell lines (denoted as HSC70 KO) using CRISPR-Cas9. The knockout of HSC70 was confirmed by screening various clones by immunoblotting (Fig. S5*A*). HSC70 KO cells also showed a significant reduction in the colocalization of ARL5B with Golgin-97, as quantified using Motion tracking (Fig. 3, *A* and *B*) and correlation analysis by ImageJ (Fig. S5*B*). We ensured that the overall Golgi morphology remained unaltered in HSC70 KO cells by immunostaining the cells with Golgin-97 and measuring the Golgi area (Fig. S5, *C* and *D*) (33). The quantification of the Golgi area revealed no significant difference in the Golgi area of control and HSC70 KO cells (Fig. S5*D*). To further strengthen our results, we assessed the Golgi-associated levels of ARL5B by extracting the Golgi from control and HSC70 KO MDA-MB-231 cells by sucrose density gradient centrifugation. In line with our localization studies, we observed significantly reduced levels of ARL5B in the Golgi extracted from HSC70 KO cells (78% reduction) compared with the control cells (Fig. 3, *C* and *D*). We next analyzed the level of ARL5B in control and HSC70 KO cells to rule out whether the decrease in the Golgi-associated level of ARL5B is due to the overall reduction in the total level of ARL5B. We observed that in contrast to the case of siRNA-mediated depletion of HSC70, the total level of ARL5B in HSC70 KO cells was comparable to the control cells (Fig. S5, *E* and *F*). The difference in the expression level of ARL5B in HSC70 knockdown cells compared with the HSC70 KO cells may be due to a compensatory mechanism in HSC70 KO cells.

To further validate our findings and ensure the gene-specific effect, we performed a rescue experiment with wild-type and ATPase-deficient mutant (HSC70K71M) (34) of HSC70. Although the overexpression of GFP-HSC70 in HSC70 KO cells could partially rescue the localization of ARL5B with Golgin-97, the overexpression of GFP-HSC70K71M could not (Fig. 3, *E* and *F*), suggesting that the ATPase function of HSC70 is important for the Golgi localization of ARL5B. Due to the technical limitations in the object identification of ARL5B in overexpressing cells, we performed the pixel intensity-based correlation analysis alone.

Next, we investigated whether the involvement of HSC70 in the membrane localization is specific for ARL5B. We first checked whether other ARF family members, including ARL5A (another paralog of ARL5 in humans and 79.89% identical to ARL5B), ARF1 (49.17% identical to ARL5B), ARF6 (43.02% identical to ARL5B), and ARL4A (38.50% identical to ARL5B) could also bind to HSC70 (Fig. S6*A*). By virtue of the presence of hydrophobic and basic amino acids in the N-terminus (ARL5B and ARL5A) or by the presence of KFERQ-like motifs (ARF1, ARF6, and ARL4A) (35), we observed that these proteins also could pull down HSC70 (Fig. S6, *B* and *C*). Further, to address the functional specificity of the interaction, we examined the localization of two Golgi-localized ARF family members, ARL5A and ARF1. We overexpressed ARL5A-GFP and ARF1-GFP in control and HSC70 knockout MDA-MB-231 cells and immunostained for Golgi markers. Strikingly, we observed that the knockout of HSC70 did not affect the Golgi localization of ARL5A or ARF1, indicating a specific role of HSC70 on the localization of ARL5B (Fig. S7, *A*–*D*). As the functional specificity in HSP70 family members is brought about by J domain-containing proteins, we also checked whether the depletion of GAK, a J domain protein associated with Golgi (36), affects the localization of ARL5B. However, we observed that the siRNA-mediated knockdown of GAK did not affect the localization of ARL5B with Golgi (Fig. S7, *E*–*G*). Altogether, these results indicated a novel role of HSC70 in the Golgi localization of ARL5B.

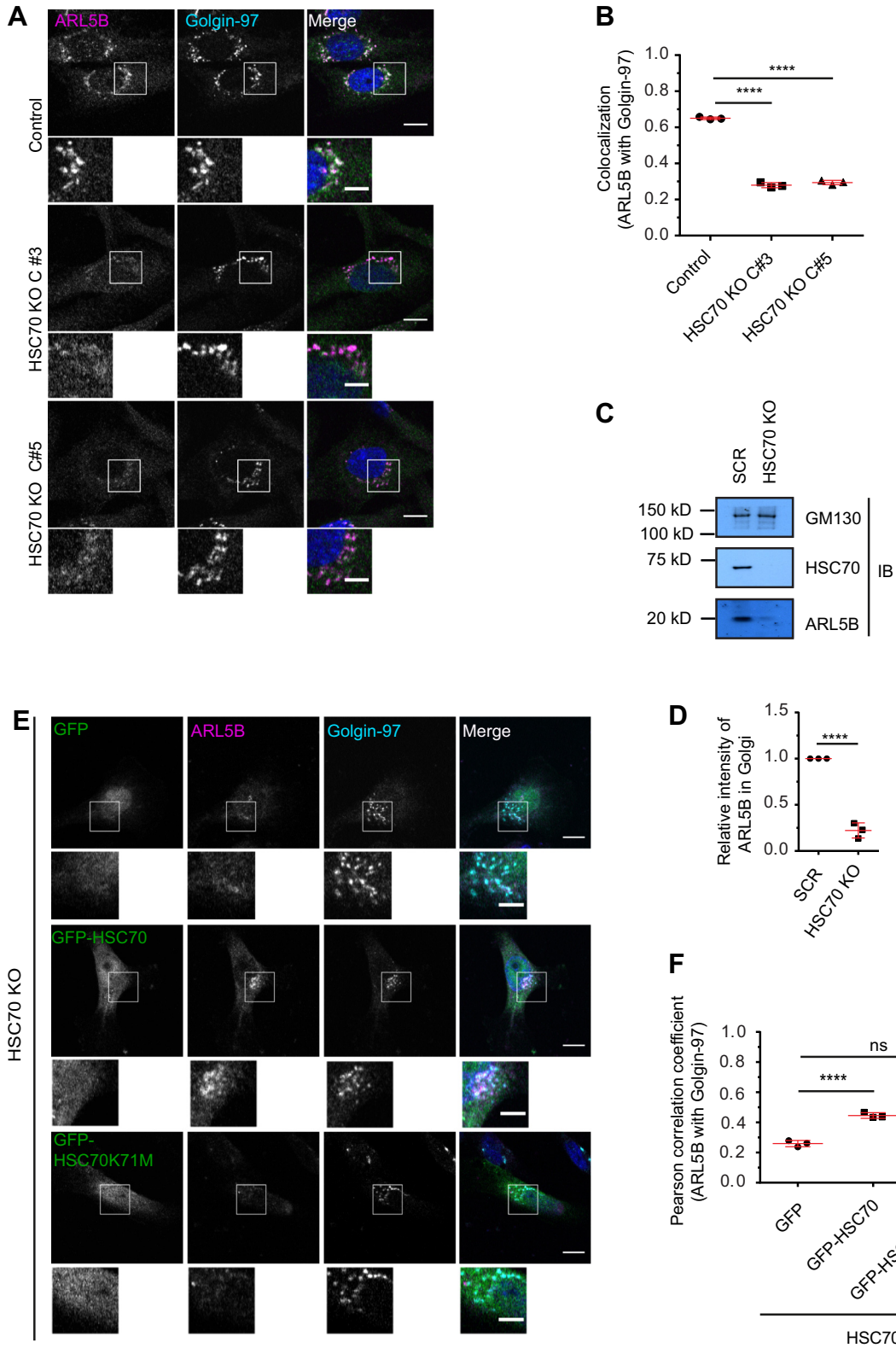

Figure 3. The Golgi localization of ARL5B is reduced in HSC70 knockout cells. *A*, control and HSC70 knockout (HSC70 KO) MDA-MB-231 cells were fixed and immunostained using ARL5B and Golgin-97 antibodies. The nucleus was labeled using DAPI, and images were acquired by a confocal microscope. Scale bars: 10 μm. Zoomed in area is shown at the *bottom*. Scale bars: 5 μm. *B*, the graph shows colocalization expressed as the ratio of the integral intensity of colocalized objects (ARL5B and Golgin-97) to integral intensity of the total objects found in ARL5B, measured using Motion tracking software. Data are mean ± SD, n = 3, >200 cells analyzed per condition. The colocalization values are: Control - 0.65 ± 0.00, HSC70 KO#3 – 0.27 ± 0.01, HSC70 KO#5 – 0.29 ± 0.01. Statistical significance was calculated using One-way ANOVA, **** $p < 0.0001$. *C*, Golgi extracted from control and HSC70 knockout MDA-MB-231 cells were analyzed by immunoblotting using anti-GM130, anti-HSC70, and anti-ARL5B antibodies. *D*, the graph shows the quantification of the relative intensity of ARL5B in Golgi extracted from control and HSC70 KO cells (*panel C*) by densitometric analysis from three independent experiments. Values are mean ± SD. Statistical significance was calculated using an unpaired two-tailed Student's *t* test, **** $p < 0.0001$. *E*, GFP, GFP-HSC70, or GFP-HSC70K71M was

HSC70 controls the Golgi association of ARL5B in vitro

To investigate whether HSC70 could directly participate in the Golgi localization of ARL5B and if it depends on the nucleotide status of the small GTPase, we employed an *in vitro* reconstitution approach. GDP or GTP loaded His-ARL5B was myristoylated *in vitro* as previously described (37). Myristoylation adds 221 Da to the protein, leading to a slight downward shift in the mobility of the proteins (37–41). We ran the samples before and after *in vitro* myristoylation on a 10% Tricine-SDS-PAGE (Fig. S8*A*), as Tricine-SDS-PAGE offers a better resolution for the separation of proteins that are smaller than 30kD (42). Since the proteins were His-tagged, we also ran the samples on a 15% SDS-PAGE and analyzed them by immunoblotting using an anti-His antibody (Fig. S8*B*). We observed that the myristoylated protein is indeed downshifted (Fig. S8, *A* and *B*). We then confirmed the myristoylated proteins to be functional by checking their ability to exchange nucleotides using fluorescence-based assay (Fig. S8*C*). We also checked whether the myristoylated proteins could associate with the purified Golgi membrane (Fig. S8, *D* and *E*). While the GTP-loaded myr-His-ARL5B could associate significantly more with the Golgi membrane than the GDP-loaded GTPase, [ΔN15]ARL5B, incapable of being myristoylated, failed to associate with the purified Golgi membrane.

Next, we analyzed the binding of GDP and GTP-loaded myr-ARL5B to the purified Golgi membrane in either the absence or presence of HSC70. We observed a significant increase in the Golgi association for both GDP and GTP loaded myr-ARL5B in the presence of HSC70, suggesting that HSC70 promotes the Golgi association of myr-ARL5B *in vitro* (Figs. 4, *A* and *B* and S8, *F* and *G*). Although we observed the effect for both the nucleotide-bound forms of ARL5B, it was more pronounced for myr-ARL5B-GDP than for myr-ARL5B-GTP (Figs. 4, *A* and *B* and S8, *F* and *G*). The addition of HSC70 increased the Golgi association of myr-ARL5B-GDP by 2.55-fold and myr-ARL5B-GTP by 1.75-fold (Fig. 4*B*).

To better mimic the physiological condition and examine whether other factors from the cytosol participate in the Golgi association of ARL5B, we included cytosol in the reaction. We extracted cytosol from HSC70 knockout HeLa cells. The cytosol fractions were analyzed by immunoblotting using an anti-GAPDH antibody (Fig. 4*C*). We first assessed the Golgi binding of myr-ARL5B-GDP and myr-ARL5B-GTP in the presence and absence of cytosol. In agreement with the previous studies (5, 43), we observed that the GTP-loaded myr-ARL5B associated significantly more with the Golgi than the GDP-loaded myr-ARL5B, and the Golgi association was more when the reaction was performed in the presence of cytosol (Fig. S9, *A* and *B*). Further, we incubated GDP and GTP-loaded myr-ARL5B with Golgi membrane in the presence of cytosol extracted from control or HSC70 KO cells. Interestingly, the addition of HSC70-depleted cytosol increased the Golgi association of myr-ARL5B-GDP while there was no significant change for myr-ARL5B-GTP. Supplementing recombinant HSC70 in the reaction mix containing HSC70-depleted cytosol did not significantly affect the association (Figs. 4, *D* and *E* and S9, *C* and *D*). The quantification showed that the addition of HSC70 KO cytosol increased the Golgi association of myr-ARL5B-GDP by 1.39 times (Fig. 4*E*). This result implied that in the presence of unknown cytosolic factor/factors, HSC70 shows specificity for myr-ARL5B-GDP and inhibits its association with Golgi. Hence, overall these results suggest that in the presence of other cellular factors, HSC70 preferentially binds to the GDP-bound form of ARL5B and affects its Golgi association.

HSC70-ARL5B interaction contributes to the intracellular distribution of CIMPR

As the proper localization of a GTPase is critical for their functioning, we next carried out experiments to examine how HSC70-ARL5B interaction affects the Golgi-associated functions of ARL5B. ARL5B is known to regulate the transport between Golgi and the endosomes (13, 15, 18), and cation-independent mannose-6-phosphate receptor (CIMPR) is a well-established cargo studied in the endosome-Golgi route (44). We first examined the intracellular distribution of CIMPR in MDA-MB-231 cells treated with siRNA targeting ARL5B. We confirmed the knockdown efficiency of ARL5B siRNA by qRT-PCR (Fig. S10*A*). The cells treated with ARL5B siRNA were fixed, immunostained using anti-CIMPR and anti-Golgin-97 antibodies, and imaged using a laser scanning confocal microscope. We observed that the colocalization of CIMPR with Golgin-97 was significantly increased in ARL5B-depleted cells (Fig. S10, *B* and *C*). Next, to rule out off-target effects, we generated ARL5B knockout MDA-MB-231 cell lines (denoted as ARL5B KO) using CRISPR-Cas9. The knockout of ARL5B was confirmed by screening various clones by immunoblotting (Fig. S10*D*). Immunostaining in ARL5B KO MDA-MB-231 cells revealed that the colocalization of CIMPR with Golgin-97 was significantly increased in ARL5B KO cells (∼37%) compared with the control cells (∼14%) (Fig. 5, *A* and *B*). We also validated the result in a different clone of ARL5B knockout (Fig. S10, *E* and *F*). Likewise, we checked whether the depletion of HSC70 exhibited a similar phenotype. We observed that the colocalization of CIMPR with Golgin-97 increased to 27% in HSC70 KO MDA-MB-231 cells (Fig. 5, *A* and *B*). Furthermore, we noted that the distribution of CIMPR in ARL5B knockout cells treated with HSC70 siRNA was comparable to that observed in ARL5B KO cells (Fig. 5, *A* and *B*).

Having established that the N-terminal helix and the nucleotide status of ARL5B contribute to the recognition by

overexpressed in HSC70 knockout MDA-MB-231 cells. The cells were fixed and immunostained using ARL5B and Golgin-97 antibodies. The nucleus was labeled using DAPI, and images were acquired by a confocal microscope. Scale bars: 10 μm. Zoomed in area is shown at the *bottom*. Scale bars: 5 μm. *F*, the graph shows the Pearson correlation coefficient measured using ImageJ. Data are mean ± SD, n = 3, >60 cells analyzed per condition. The colocalization values are: GFP – 0.25 ± 0.02, GFP-HSC70 – 0.44 ± 0.01, GFP-HSC70K71M – 0.22 ± 0.02. Statistical significance was calculated using One-way ANOVA, **** $p <$ 0.0001, ns $p > 0.05$.

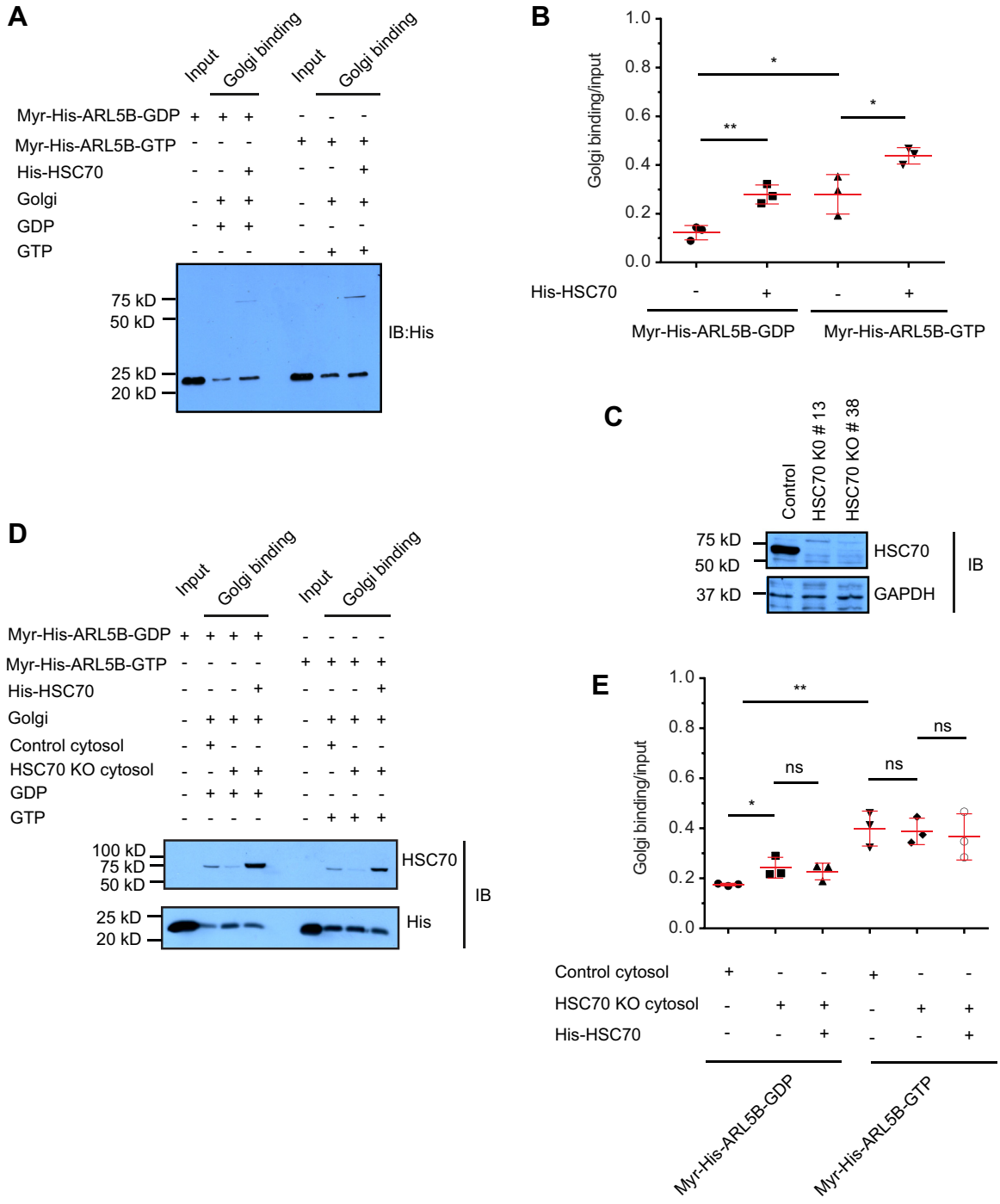

Figure 4. HSC70 fine-tunes the Golgi binding of GDP loaded myr-ARL5B. *A*, representative immunoblot showing the Golgi binding of 1 μM of myr-ARL5B-GDP or myr-ARL5B-GTP, in the presence and absence of 0.5 μM of HSC70. The reaction was performed in the presence of 5 mM ADP and 1 mM of GDP/GTP. *B*, the relative Golgi binding of ARL5B was quantified by densitometric analysis of immunoblots from three independent experiments. Other blots used for quantification are shown in Figure S8, *F* and *G*. Values are mean ± SD. Statistical significance was calculated using an unpaired two-tailed Student's *t* test, * $p < 0.05$, ** $p < 0.01$. *C*, cytosol purified from control and HSC70 KO HeLa cells was analyzed by immunoblotting using anti-GAPDH and anti-HSC70 antibodies. *D*, representative immunoblot showing the Golgi binding of 1 μM of myr-ARL5B-GDP or myr-ARL5B-GTP in the presence of cytosol from control and HSC70 KO cells. The reaction was performed in the presence of 5 mM ADP and 1 mM of GDP/GTP. *E*, the relative Golgi binding of ARL5B was quantified by densitometric analysis of immunoblots from three independent experiments. Other blots used for quantification are shown in Figure S9, *C* and *D*. Values are mean ± SD. Statistical significance was calculated using an unpaired two-tailed Student's *t* test, * $p < 0.05$, ns $p > 0.05$.

HSC70 (Fig. 2, *A*–*F*), we next tested whether the overexpression of GFP-tagged wild-type ARL5B, constitutively active ARL5B (ARL5BQ70L), dominant negative ARL5B (ARL5BT30N), and [ΔN15]ARL5B could rescue the distribution of CIMPR in ARL5B KO cells. The overexpression of ARL5B-GFP and ARL5BQ70L-GFP in ARL5B KO cells significantly reverted the Golgi distribution of CIMPR (Fig. 5, *C* and *D*). However, ARL5BT30N-GFP, being an inactive mutant and [ΔN15]ARL5B-GFP, being unable to localize to Golgi, could not rescue the distribution of CIMPR (Fig. 5, *C*

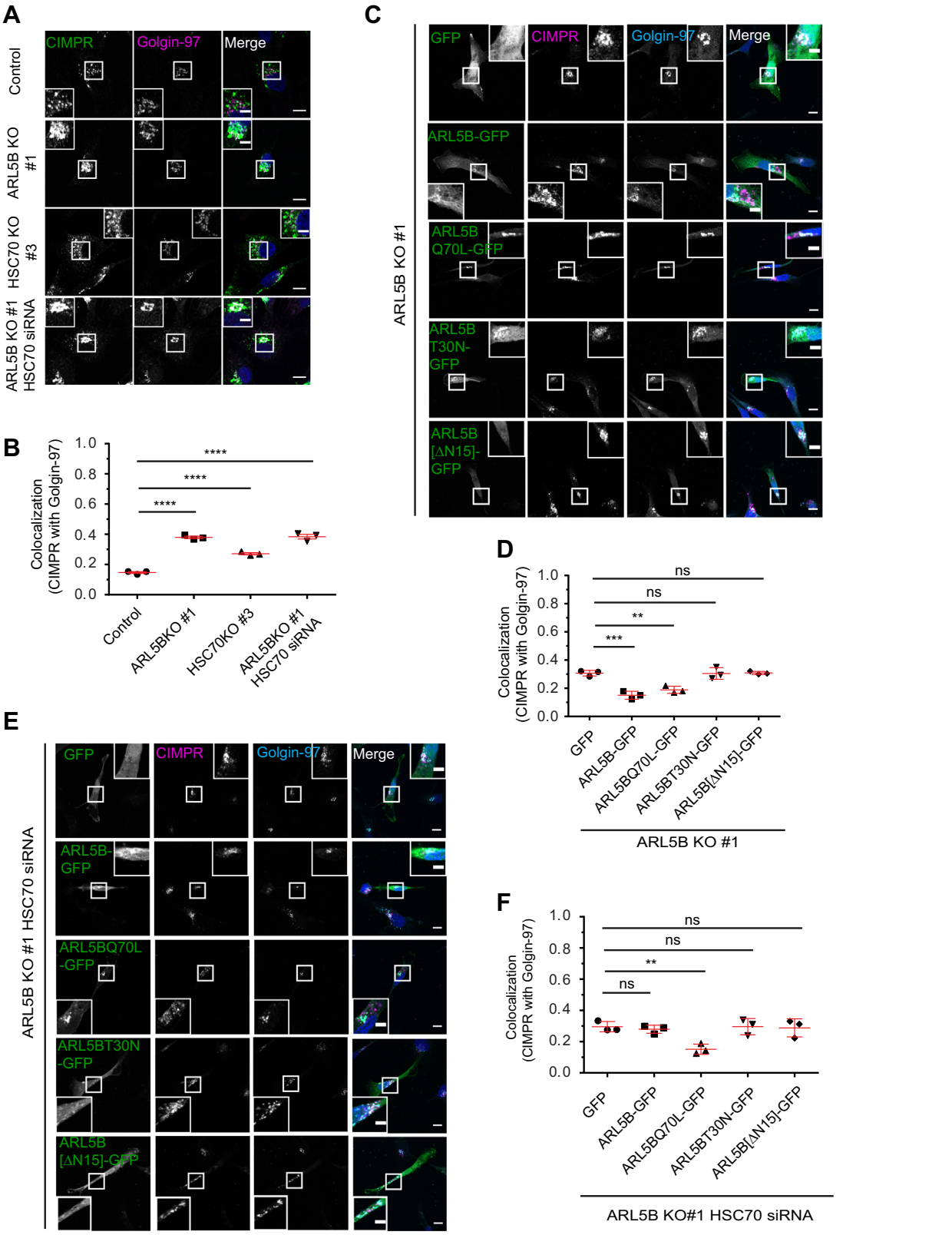

Figure 5. HSC70-ARL5B interaction affects the distribution of CIMPR. *A*, control, ARL5B knockout (ARL5B KO #1), HSC70 knockout (HSC70 KO #3), and ARL5B KO cells treated with HSC70 siRNA (ARL5B KO #1 HSC70 siRNA) were fixed and immunostained using CIMPR and Golgin-97 antibodies. The nucleus was labeled using DAPI, and images were acquired by a confocal microscope. Scale bars: 10 μm. Inset scale bars: 5 μm. *B*, the graph shows the object-based colocalization measured using Motion tracking software. Data are mean ± SD, n = 3, >200 cells analyzed per condition. Colocalization values are: Control – 0.14 ± 0.01, ARL5B KO#1 – 0.37 ± 0.01, HSC70 KO #3 – 0.27 ± 0.01, ARL5B KO#1 HSC70 siRNA – 0.38 ± 0.02. Statistical significance was calculated using One-way ANOVA, **** $p < 0.0001$. *C*, GFP, ARL5B-GFP, ARL5BQ70L-GFP, ARL5BT30N-GFP, and ARL5B[ΔN15]-GFP were overexpressed in ARL5B knockout MDA-MB-231 cells. The cells were fixed and immunostained using CIMPR and Golgin-97 antibodies. The nucleus was labeled using DAPI, and images were acquired by a confocal microscope. Scale bars: 10 μm. Inset scale bars: 5 μm. *D*, the graph shows the object-based colocalization measured using Motion

and *D*). To further strengthen our results and demonstrate the relevance of ARL5B-HSC70 interaction, we performed rescue experiments in ARL5B KO cells treated with HSC70 siRNA. Before proceeding, we checked whether HSC70 affects the Golgi localization of GFP-tagged wild-type ARL5B, ARL5BQ70L, and ARL5BT30N. The depletion of HSC70 significantly affected the Golgi localization of wild-type ARL5B and ARL5BT30N, whereas the localization of ARL5BQ70L was unaffected (Figs. S10, *G* and *H* and 3, *B* and *C*). In corroboration, we observed that the overexpression of ARL5BQ70L-GFP in ARL5B KO cells treated with HSC70 siRNA could significantly rescue the distribution of CIMPR, whereas the overexpression of wild-type ARL5B-GFP could not (Fig. 5, *E* and *F*). Our results indicated that HSC70 plays a role in ARL5B-mediated Golgi distribution of CIMPR.

Discussion

ARL5B is previously shown to regulate the transport of cargoes between the Golgi and endosomes by recruiting proteins such as Adaptor protein complex; AP4, Golgi-associated retrograde protein (GARP), and Lamtor1, a subunit of Ragulator (13, 15, 18). In the current study, we have identified HSC70, a constitutively expressed chaperone, as an interacting partner of ARL5B. Using biochemical and biophysical approaches, we have shown that HSC70 binds to ARL5B in the presence of ADP, which indicates that ARL5B is a substrate of HSC70 (Fig. 1, *D–G*). The N-terminal helix of ARL5B contains hydrophobic residues and no acidic residues, which indeed qualify the requirement for being a substrate for HSC70 (26, 27). Accordingly, we found that the interaction of HSC70 with ARL5B was abolished when the first 15 residues in the N-terminal of ARL5B were deleted (Fig. 2, *A–D*). Earlier, chaperones such as RABIF/MSS4 (mammalian suppressor of yeast Sec4) and BAG6 (also called BAT3 or Scythe) were also shown to recognize the exposed hydrophobic residues in Rabs (45, 46). While BAG6 prevents the excessive accumulation of inactive Rabs, RABIF/MSS4 promotes the stability of Rabs (45, 46). Although we attempted to point out the residues in the N-terminal of ARL5B that are important for the recognition by HSC70, we were not successful (Fig. S2, *E–J*). Prior studies using peptide library also concur with our result that members of the HSP70 family do not recognize a specific binding motif but a stretch of 5 to 7 hydrophobic residues (26, 47). Hence, it is likely that multiple hydrophobic residues in the patch contribute together, and point mutations would not significantly perturb the interaction.

The myristoyl group and the hydrophobic residues in the N-terminal helix of the ARF family members are important for their membrane association (5). In corroboration, the deletion of 15 amino acids from the N-terminal of ARL5B affected its association with Golgi (Fig. S8*E*) and the protein localized to cytoplasm and nucleus (Fig. S2*C*). The deletion of the amphipathic helix of ARLs such as ARFRP1and ARL14 or mutations in the myristoylation site of ARL5B and ARL1 was previously shown to have a similar localization (18, 48, 49).

Using cellular studies, we have shown that the depletion of HSC70 reduces the Golgi localization of ARL5B (Figs. 3, *A–D*, S4, *C–F* and S5*B*). Previously, HSP-1 (homolog of HSC70 in *Caenorhabditis elegans*) was shown to associate with and inhibit the localization of leucine-rich repeat kinase, LRK-1 to the Golgi and thus determining polarized sorting of synaptic vesicle proteins to axons (50). Contrarily, here we show that HSC70 assists the Golgi localization of ARL5B (Figs. 3, *A–D*, S4, *C–F* and S5*B*). Owing to the presence of hydrophobic and basic residues in the N-terminal or the presence of KFERQ-like motifs, other ARF family members, including ARL5A, ARF1, ARF6, and ARL4A, also could interact with HSC70 (Fig. S6, *A–C*). This result is in line with the fact that HSC70 has a broad range of substrates *in vitro* (51). However, unlike ARL5B, the Golgi localization of ARL5A and ARF1 was unaffected by HSC70 knockout, which emphasizes the specificity in the function of HSC70 (Fig. S7, *A–D*). We believe that the specific effect of HSC70 on the localization of ARL5B and not ARL5A or ARF1 is possibly mediated by a J-domain containing protein. This is well supported by the fact that even though HSC70 binds to a wide range of substrates *in vitro* (51), the functional diversity of the HSP70 chaperone machinery in the cell is provided mainly by J domain proteins (52). This is also evident from the large multiplicity of J domain proteins for a minimal number of HSP70 family members (52). J domain-containing proteins stimulate ATP hydrolysis and affect the binding of HSP70 family members with its substrates. Many J proteins interact with the same HSP70 to carry out a multitude of functions (53). Through the localization to a specific site of action or by specific binding to the substrates, J domain proteins bring about the specificity in functions of the HSP70 family of chaperones (52). In an attempt to find the J protein, we tested the role of GAK, a J protein localized on Golgi (36), in affecting the localization of ARL5B. However, the depletion of GAK did not affect the Golgi localization of ARL5B (Fig. S7, *E–G*). As GAK acts as a cochaperone of HSC70 in uncoating clathrin-coated vesicles produced at trans-Golgi (36), it hints that the effect on Golgi localization of ARL5B may not be a consequence of HSC70's role in uncoating clathrin-coated vesicles. It is likely that a distinct J protein renders specificity for HSC70. Further studies should be sought to identify the J protein and decipher the specificity underlying the HSC70-mediated Golgi localization of ARL5B.

tracking software. Data are mean ± SD, n = 3, >60 cells analyzed per condition. The colocalization values are: GFP – 0.30 ± 0.02, ARL5B-GFP – 0.15 ± 0.02, ARL5BQ70L-GFP – 0.18 ± 0.02, ARL5BT30N-GFP – 0.30 ± 0.04, ARL5B[ΔN15]-GFP – 0.30 ± 0.01. Statistical significance was calculated using One-way ANOVA, *** $p < 0.001$, ** $p < 0.01$, ns $p > 0.05$. *E*, GFP, ARL5B-GFP, ARL5BQ70L-GFP, ARL5BT30N-GFP, and ARL5B[ΔN15]-GFP were overexpressed in ARL5B knockout MDA-MB-231 cells treated with HSC70 siRNA. The cells were fixed and immunostained using CIMPR and Golgin-97 antibodies. The nucleus was labeled using DAPI, and images were acquired by a confocal microscope. Scale bars: 10 μm. Inset scale bars: 5 μm. *F*, the graph shows the object-based colocalization measured using Motion tracking software. Data are mean ± SD, n = 3, >60 cells analyzed per condition. Colocalization values are: GFP – 0.29 ± 0.03, ARL5B-GFP – 0.15 ± 0.03, ARL5BQ70L-GFP – 0.19 ± 0.01, ARL5BT30N-GFP – 0.29 ± 0.05, ARL5B[ΔN15]-GFP – 0.28 ± 0.05. Statistical significance was calculated using One-way ANOVA, ** $p < 0.01$, ns $p > 0.05$.

The results from pull-down assay using GDP/GTP loaded His-ARL5B and MDA-MB-231 cell lysate showed that HSC70 is pulled down preferentially with GDP loaded ARL5B (Fig. 2*F*). Similarly, when we performed a nanobody-based GBP pull-down using the lysate from cells expressing ARL5BQ70L-GFP (GTP restricted) and ARL5BT30N-GFP (GDP restricted), we observed that HSC70 bound relatively more with ARL5BT30N, the GDP-restricted mutant of ARL5B (Figs. 2, *E* and *F* and S3, *A* and *B*). Therefore, in addition to the N-terminal helix (Fig. 2, *A–D*), the nucleotide status of ARL5B also contributes to the recognition by HSC70 (Figs. 2, *E* and *F* and S3, *A* and *B*). However, when bacterially expressed and purified GST-HSC70 was incubated with purified His-ARL5B, GST-HSC70 bound equally with both GDP and GTP loaded ARL5B (Fig. S3, *D–F*). This result indicates that HSC70 preferentially binds to the GDP-bound form of ARL5B in the presence of other cellular factors. The preference of HSC70 for the GDP bound form of ARL5B was also corroborated by the results from *in vitro* reconstitution experiments. In the absence of cytosol, the addition of recombinant HSC70 (His-HSC70) significantly enhanced the Golgi association of both GDP and GTP-loaded myr-ARL5B (Figs. 4, *A* and *B* and S8, *F* and *G*). Of note, the effect was more pronounced for myr-ARL5B-GDP (Figs. 4, *A* and *B* and S8, *F* and *G*). On the other hand, when the reactions were performed in the presence of control/HSC70 KO cytosol, the addition of HSC70-depleted cytosol increased the Golgi association of myr-ARL5B-GDP while there was no significant change for myr-ARL5B-GTP (Figs. 4, *D* and *E* and S9, *C* and *D*). Taken together, these results indicate that in the presence of other cellular factors, HSC70 binds preferentially to the GDP-bound form of ARL5B and controls its Golgi association.

Our findings indicated that HSC70 shares some features with GDI. First, like GDIs, HSC70 is bound preferentially to the GDP-bound form of the GTPase (Figs. 2, *E* and *F* and S3, *A* and *B*). Second, HSC70 binds to the N-terminal helix of ARL5B (Fig. 2, *A–D*), which is myristoylated and important for membrane association (Figs. S8*E* and S2*C*). Likewise, GDIs bind to and shield the hydrophobic prenyl moiety at the C-terminal of the GTPase, which is important for membrane targeting (9). We believe that HSC70 binds to the GDP-bound form of ARL5B and potentially shields the myristoyl modification and the hydrophobic residues in the N-terminal helix from the aqueous cytosol. Third, depending on the relative proportion of HSC70 and the Golgi membrane, HSC70 was able to facilitate as well as inhibit the Golgi association of ARL5B-GDP (Figs. 4, *A*, *B*, *D* and *E*, S8, *F* and *G* and S9, *C* and *D*). Similarly, the GDI for Rab9 was previously reported to have the ability to solubilize Rab9 in the cytosol as well as to recycle Rab9 back to the membrane, thus regulating the endosome-TGN trafficking (54, 55). The seeming discrepancy observed in the result of *in vitro* reconstitution experiment using cytosol (Figs. 4, *D* and *E* and S9, *C* and *D*) with the results from microscopy (Figs. 3, *A* and *B*, S4, *C* and *F* and S5*B*), cell fractionation (Fig. 3, *C* and *D*), and the cytosol-free *in vitro* reconstitution experiments (Figs. 4, *A* and *B* and S8, *F* and *G*) could also possibly arise from the difference in the relative proportion of HSC70, ARL5B, and the Golgi membrane.

An earlier study had shown that siRNA-mediated depletion of ARL5B alters the intracellular distribution of CIMPR in HeLa cells (13). Here, we found that the depletion of ARL5B in MDA-MB-231 cells increases the colocalization of CIMPR with trans-Golgi, indicative of the role of ARL5B in regulating the anterograde transport of CIMPR (Figs. 5, *A* and *B* and S10, *B*, *C*, *E* and *F*). This was further supported by the results from the rescue experiments in ARL5B KO cells, where both the wild-type and the GTP-restricted form of ARL5B could significantly revert back the distribution of CIMPR (Fig. 5, *C* and *D*). Interestingly, the distribution of CIMPR was rescued more when the wild-type ARL5B was overexpressed compared with when the mutant was overexpressed (Fig. 5, *C* and *D*), suggesting that the GTPase cycle may contribute to the proper functioning of the GTPase under physiological conditions. Of note, the effect of ARL5B KO on the distribution of CIMPR was more pronounced than the effect of HSC70 KO in MDA-MB-231 cells (Fig. 5, *A* and *B*). Moreover, we did not observe a further increase in the Golgi localization of CIMPR upon depletion of HSC70 in ARL5B KO cells (Fig. 5, *A* and *B*). These observations led us to hypothesize that the effect of HSC70 on the distribution of CIMPR is likely to be mediated by altering the Golgi localization of ARL5B in MDA-MB-231 cells.

We observed that the GTP-restricted mutant ARL5BQ70L can localize to the Golgi even in the absence of HSC70 (Fig. S10, *G* and *H*). Accordingly, the overexpression of ARL5BQ70L-GFP rescued the distribution of CIMPR in both ARL5B KO cells and HSC70-depleted ARL5B KO cells (Fig. 5, *C–F*). In contrast, the wild-type ARL5B cycles between a membrane-associated GTP-bound form and a cytosolic GDP-bound form. HSC70 preferentially associates with the GDP-bound form of ARL5B (Fig. 2*F*). Consequently, in the absence of HSC70, the delivery of the cytosolic GDP-bound ARL5B to the Golgi is affected. This explains why the overexpression of wild-type ARL5B-GFP failed to rescue the distribution of CIMPR in HSC70-depleted ARL5B KO cells (Fig. 5, *C–F*). HSC70 interacts with the GDP-restricted mutant of ARL5B (ARL5BT30N) (Fig. 2*E*); however, ARL5BT30N cannot be activated by GEF and therefore cannot carry out downstream functions. Accordingly, the overexpression of ARL5BT30N-GFP could not rescue the distribution of CIMPR (Fig. 5, *C–F*). [ΔN15]ARL5B cannot localize to the Golgi membrane as the myristoyl modification, and the N-terminal amphipathic helix important for membrane association is absent (Figs. 2, *A–D*, S2*C* and S8*E*). As a result, the overexpression of [ΔN15]ARL5B-GFP could not rescue the distribution of CIMPR (Fig. 5, *C–F*).

In summary, this study demonstrates that HSC70 interacts with the cytosolic GDP-bound form of ARL5B through the latter's N-terminal helix and helps in the delivery to the Golgi membrane, where the GTPase carries out its downstream functions (Fig. 6).

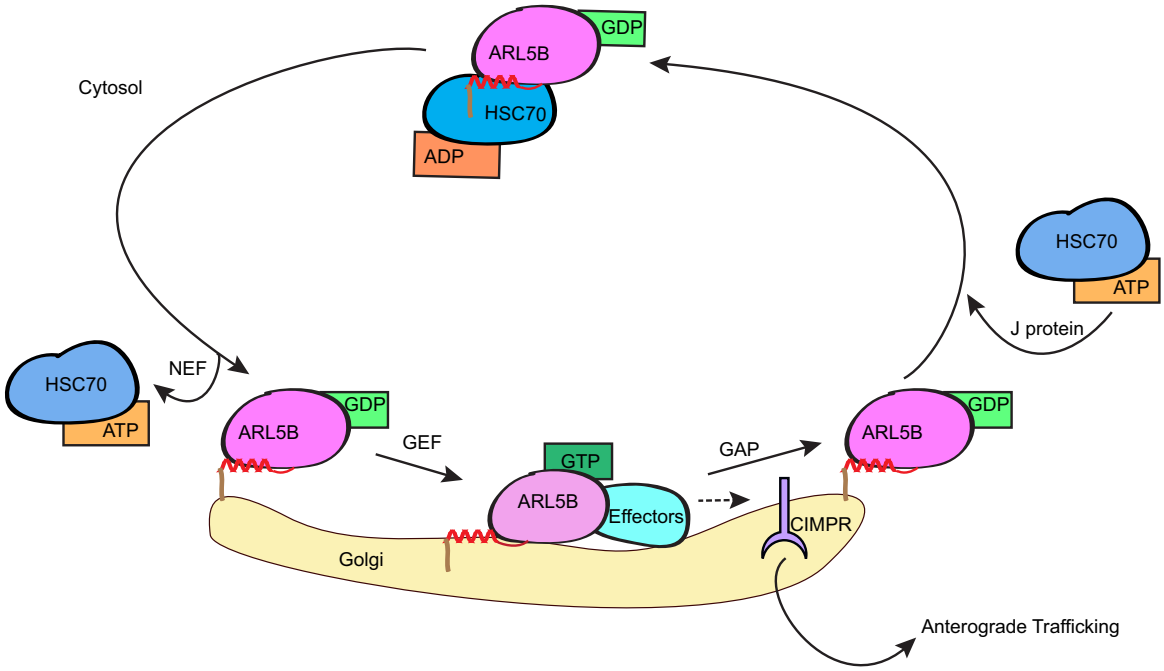

Figure 6. Proposed model for HSC70-mediated Golgi association of ARL5B. HSC70, in its ADP-bound form, recognizes the N-terminal helix of the cytosolic GDP-bound form of ARL5B and facilitates its delivery to the Golgi membrane. At the membrane, a GEF activates ARL5B allowing its interaction with the effectors and thereby governing the anterograde trafficking of CIMPR. Finally, a GAP inactivates the GTPase by accelerating its conversion to the GDP bound form. The ATPase cycle of HSC70 is regulated by Nucleotide Exchange Factors (NEFs) that facilitate the exchange of ATP to ADP, and J proteins, which stimulate ATP hydrolysis.

Experimental procedures

Cell culture

MDA-MB-231 cells (ATCC) were cultured at 37 °C in L-15 medium (Gibco) with 10% fetal bovine serum, 100 μg/ml penicillin, and 100 μg/ml streptomycin. HeLa and HEK cells were cultured in DMEM medium (Gibco) with 10% fetal bovine serum, 100 μg/ml penicillin, and 100 μg/ml streptomycin at 37 °C, 5% CO_2.

Constructs and antibodies

pGEX6P1-GFP-Nanobody was purchased from Addgene (#61838, deposited by Kazuhisa Nakayama). ARL5B-GFP was cloned in pLVX-TRE3G vector (Takara) for mammalian expression and in pET28a vector for bacterial expression using the ARL5B-GFP construct as a template (a kind gift from Prof. Sean Munro, MRC Laboratory of Molecular Biology). ARL5BQ70L-GFP and ARL5BT30N-GFP were kind gifts from Prof. Paul Gleeson (The University of Melbourne). All mutants of ARL5B were generated by site-directed mutagenesis using pET28a-ARL5B as a template. ARL5A was cloned in pEGFPN1 and pET28a using pDSHA-ARL5A-Myc as a template (#67357, deposited by Richard Kahn). GFP-HSC70K71M was generated by site-directed mutagenesis using GFP-HSC70 as a template (Addgene plasmid # 19487, deposited by Harm Kampinga). HsNMT1 was cloned in pET28a using pMON-HsNMT1 (Addgene plasmid #67475, deposited by Richard Kahn) as a template.

The antibodies used in this study are anti-mouse ARL5B (sc393511, Santa Cruz Biotechnology), anti-mouse HSC70 (sc-7298, Santa Cruz Biotechnology), anti-mouse GFP (11814460001, Roche), anti-mouse His (MA1-21315, Invitrogen), anti-mouse actin (sc47778, Santa Cruz Biotechnology), anti-rabbit Giantin (ab24586, Abcam), anti-rabbit Golgin97 (D8P2K, Cell Signaling Technology), anti-mouse transferrin receptor (13-6800, Invitrogen), anti-mouse Vinculin (V9131, Sigma-Aldrich), anti-mouse GM-130 (610822, BD Transduction Laboratories), anti-mouse syntaxin-6 (610635, BD Transduction Laboratories), anti-mouse Rab5 (610724, BD Transduction Laboratories), anti-rabbit GAPDH (A300-640A, Bethyl Laboratories; a kind gift from Dr Varun Chaudhary, IISER Bhopal) and anti-mouse CIMPR (ab2733, Abcam).

Recombinant protein expression and purification

The plasmid encoding His-ARL5B, His-[ΔN15]ARL5B, His-ARL5BK7E, His-ARL5BL8A, His-ARL5BF12A, His-ARL5BL8AF12A, His-ARL5A, His-ARL5BQ15A, His-ARL5BQ15AE16A, His-ARL5BQ15AK18A, His-HSC70, His-ARF1, His-ARF6, His-ARL4A, His-hNMT1, GST, GST-GBP, and GST-HSC70 was expressed in BL21, DE3 *E. coli* cells. A single colony was inoculated in 1 L LB broth containing 30 μg/ml kanamycin and grown at 37 °C till the OD at 600 nm reached 0.6. Further, the culture was induced with 300 μM of IPTG and grown at 16 °C overnight at a speed of 160 rpm. The cells were harvested (5000 rpm for 15 min), the pellet was washed and lysed in lysis buffer containing 50 mM Tris pH 8.0, 500 mM NaCl, 10 mM Imidazole, 1% Triton X-100, and 10 mM β-mercaptoethanol. In total, 100 μM GDP and 5 mM $MgCl_2$ were included in the lysis buffer for purification of GTPases. In total, 2 mM $MgCl_2$ and 500 μM ATP

were included in the lysis buffer for the purification of HSC70. The lysate was then clarified by centrifuging at 18,000 rpm for 30 min at 4 °C and further purified using Ni-NTA affinity chromatography for His-tagged proteins and glutathione affinity chromatography for GST-tagged proteins.

GBP pull-down assay

In total, 25 μg of GST-GBP was allowed to bind to glutathione sepharose beads in 1X PBS for 1 h at 4 °C. Further, it was incubated with precleared lysate extracted from cells expressing GFP tagged proteins for 2 h at 4 °C. The GBP-GFP complex was purified using glutathione resin (23, 24). After three washes with a buffer containing 1X PBS, 2 mM $MgCl_2$, and 0.01% NP-40, the samples were resolved on SDS-PAGE and analyzed by silver staining or immunoblotting.

In-gel digestion

Bands were excised manually from the polyacrylamide gel (performed in three replicates) and were subjected to in-gel trypsin digestion as described previously (56, 57). Briefly, the excised bands were washed with 50 mM ammonium bicarbonate with 50%(v/v) acetonitrile (ACN), followed by 100% ACN and drying under high-speed vacuum centrifugation. Reduction with 10 mM dithiothreitol (DTT) and alkylation with 55 mM iodoacetamide were performed prior to digestion with 12.5 ng/μl trypsin (Sequencing grade, Promega) at 37 °C. Digested peptides were then extracted with ammonium bicarbonate with acetonitrile and dried under vacuum centrifugation. Dried peptides were then reconstituted with 80% ACN:20% MilliQ water, spotted on MALDI plate with a sample:matrix (α-Cyano-4-hydroxycinnamic acid) ratio of 1:1, and analyzed on a MALDI-TOF mass spectrometer (MALDI ultrafleXtreme, Bruker).

Mass analysis

Mass Spectrometry (MS) run was performed on a MALDI-TOF mass spectrometer (MALDI ultrafleXtreme, Bruker) operating in MS-positive reflector mode. MS spectra were acquired between m/z 400 and 5000 Da. Peaks with the highest intensity of each spot and with a signal-to-noise ratio (S/N) of at least 5 were automatically selected for PMF.

Peptide and protein identification using PMF

Peak list was generated using flexAnalysis 3.4 software and searched in Mascot 2.8.0. Protein identification was performed using PMF. User-defined search parameters were as follows: (i) Name and date of the sequence database searched: SwissProt_2021_03, (ii) Number of sequence entries in the database: 565254; Sequences after taxonomy filter: 20387, (iii) Specificity of protease (Trypsin): Specific, (iv) Missed cleavages permitted: 0, (v) Fixed modifications considered: None, (vi) Variable modifications considered: None, (vii) Mass tolerance for precursor ions: 1.2, (viii) Mass tolerance for fragment ions: Not applicable for PMF data, (ix) Expectation value for accepting individual spectra: <0.05, (x) Threshold score: 56.

GST pull-down assay

0.06 μM GST or GST-HSC70 was allowed to bind with glutathione sepharose beads for 40 min at 4°C. Further, it was incubated with 0.25 μM of His-ARL5B for 30 min at 4°C in a buffer containing 1X PBS with 2 mM $MgCl_2$. The samples were then washed multiple times with a wash buffer containing 1X PBS, 0.01% Triton, and 2 mM $MgCl_2$. Subsequently, the bound proteins were eluted by boiling with 1X SDS dye, and the eluates were resolved by SDS-PAGE, and the binding was detected by Western blot using anti-His and anti-HSC70 antibodies.

Immunoblotting

Cells were lysed in lysis buffer containing 50 mM Tris-HCl, pH 8.0, 150 mM NaCl, 2 mM DTT, 1% NP-40 supplemented with 10 μg ml^{-1} protease inhibitor cocktail (PIC). Cell debris was removed by centrifuging at 19,000*g* for 15 min at 4 °C. Samples were separated on SDS-PAGE and transferred to a nitrocellulose membrane (0.45 μm; GE Healthcare, Cat.10600002). The membrane was blocked with 5% BSA and incubated for 1 h at room temperature with the appropriate primary antibody. The membrane was further incubated with HRP-conjugated or fluorescently labeled secondary antibodies to detect signals using enhanced chemiluminescence (Bio-Rad) or Li-Cor Odyssey Infrared Scanning System, respectively.

His pull-down assay

In total, 25 μg of His-tagged proteins was immobilized on Ni-NTA beads and incubated with 400 μg of precleared MDA-MB-231 cell lysate for 2 h at 4°C. The unbound proteins were washed with a buffer containing 50 mM Tris pH 8.0, 150 mM NaCl, 2 mM $MgCl_2$ and 0.1% NP-40. The bound proteins were eluted by boiling with 1X SDS dye. The eluates were analyzed by immunoblotting using anti-HSC70 and anti-His antibodies.

Isothermal titration calorimetry (ITC)

ITC was performed using Nano ITC (TA Instruments). In total, 30 μM of HisARL5B was titrated into 1 μM of His-HSC70 in the presence of 5 mM ADP or ATP. The titration was carried out in a buffer containing 50 mM Tris pH8.0, 100 mM NaCl, 5 mM $MgCl_2$, and 2 mM DTT at room temperature. The raw data of interaction was processed by using NanoAnalyze software, and thermodynamic parameters were calculated.

Nucleotide exchange and HPLC analysis

For nucleotide exchange, purified His-ARL5B protein was incubated with a 50-fold excess of GDP/GTP in exchange buffer containing 25 mM HEPES pH 7.5, 100 mM NaCl, 1 mM EDTA, and 0.5 mM $MgCl_2$, 3 mM DMPC, and 0.1% sodium cholate at 30 °C for 30 min (58). The protein was passed through the NAP-5 desalting column to remove the excess nucleotide. For nucleotide analysis, the protein was boiled for 3 min at 90 °C and centrifuged at 13,000*g* for 10 min to

remove the denatured protein. The supernatant was injected into a Sunfire C-18 reversed-phase column (0.46 cm × 25 cm) filled with 5 μm (particle size) silica(Waters). The column was equilibrated with a buffer containing 100 mM KH_2PO_4(pH 6.5), 10 mM tetrabutylammonium bromide, 0.2% sodium azide (NaN_3), and 7.5% acetonitrile. Isocratic elution was performed at ambient temperature with a flow rate of 1 ml/min. The retention times of GDP and GTP were ∼4.8 min and ∼6 min, respectively. The column was calibrated using different concentrations of GDP and GTP.

Circular dichroism (CD)

The CD measurements were performed in JASCO J-815 spectropolarimeter in a buffer containing 20 mM Tris pH 8.0 and 10 mM NaCl using a cuvette of 1.0 mm path length. In total, 5 μM of each protein was used, and the data was collected from 250 to 200 nm. The analysis was done using the BeStSel (Beta Structure Selection) software (http://bestsel.elte.hu/) (59, 60).

RNA extraction and qRT-PCR

Total RNA was extracted using PureLink RNA Minikit (Invitrogen), and cDNA was prepared using High Capacity RNA to cDNA kit (Applied Biosystems). Real-time qPCR reactions were performed using the SYBR Green Kit (Applied Biosystems) and corresponding primers in Applied Biosystems 7300 Real-Time PCR System. GAPDH was used as an internal control.

siRNA transfection

MDA-MB-231 cells were transfected with negative control siRNA(denoted as SCR, D-001810-10-20), and 30 nM of individual HSC70 siRNA oligos referred to as oligo #1 (J-017609-06-0002), oligo #2 (J-017609-07-0002), oligo #3 (J-017609-08-0002), 25 nM of GAK SMARTpool siRNA (L-005005-00-0005), and 25 nM of ARL5B SMARTpool siRNA (L-017861-02-0005) using Dharmafect (GE Dharmacon) and incubated for 72 h before downstream analysis.

Cell fractionation

MDA-MB-231 cells grown in 60 mm dishes were transfected with siRNAs of SCR and HSC70 oligo #3 for 72 h. The cells were washed with ice-cold 1X PBS and snap-frozen using liquid nitrogen followed by thawing at room temperature. The cells were scraped off using lysis buffer containing 0.1 M MES-NaOH pH 6.5, 0.2 M sucrose, 1 mM magnesium acetate, 200 μM sodium orthovanadate, protease inhibitor cocktail, and centrifuged at 10,000*g* for 10 min. The supernatant (cytosol fraction) was collected, and the pellet was solubilized in lysis buffer (as mentioned above) supplemented with 1% Triton X-100, 0.1% SDS followed by centrifugation at 10,000*g* for 10 min. The supernatant from this step was collected as the membrane fraction.

Transient transfection

MDA-MB-231 cells were seeded on coverslips a day before the experiment. The cells were transfected with 0.5 μg of plasmid DNA using LTX/Plus transfection reagent (Life Technologies).

Immunofluorescence microscopy and colocalization analysis

For immunostaining using ARL5B antibody, the cells were fixed with 4% paraformaldehyde for 10 min and permeabilized for 15 min with 0.15% saponin in 1X PBS. The cells were then blocked using 0.5% BSA in 1X PBS for 30 min at room temperature. Further, the cells were incubated with the appropriate primary antibody. Following washes with 0.5% BSA in 1X PBS, the cells were coincubated with Alexa Fluor^R-conjugated secondary antibodies (Life Technologies) and DAPI (4′, 6-diamidino-2-phenylindole) for 1 h at room temperature. For immunostaining using other antibodies, the cells were fixed with 4% paraformaldehyde for 10 min and permeabilized for 12 min with 0.1% Triton in 1X PBS. The cells were then blocked using 5% fetal bovine serum (FBS) in 1X PBS for 30 min at room temperature. Further, the cells were incubated with the appropriate primary antibody. Following washes with 5% FBS in 1X PBS, the cells were coincubated with Alexa Fluor^R-conjugated secondary antibodies (Life Technologies) and DAPI (40, 6-diamidino-2-phenylindole) for 1 h at room temperature. The coverslips were mounted and imaged using a Zeiss LSM 780 Laser Scanning Confocal Microscope with a 63 × /1.4 NA oil immersion objective lens or Olympus FV3000 confocal laser-scanning microscope with a 60 × Plan Apo N objective (oil, 1.42 NA). Colocalization was calculated by an object-based automated image analysis program, Motion Tracking (http://motiontracking.mpi-cbg.de) (31, 32). Briefly, the objects were identified in each channel based on their size, fluorescence intensity, and other parameters. Colocalization was calculated as the ratio of the integral intensity of colocalized objects (*e.g.*, A to B) to the integral intensity of total objects found in A. The objects detected in two different channels were considered to be colocalized if the relative overlap of respective areas was >35%. The apparent colocalization was corrected for random colocalization. Pearson's correlation coefficient was determined after Costes' automatic threshold by using ImageJ-Fiji (61). The Golgi dispersion was measured by quantifying the area occupied by Golgin-97 staining using ImageJ-Fiji (33).

CRISPR/Cas9 knockout

The knockout cell lines were generated using CRISPR/Cas9 (Invitrogen). The sgRNAs targeting HSC70 (5′-UCGCC UUUACGGACACACUGAA-3′), ARL5B (5′-GGCUGAUCU UCGCCAAACUG-3′), and nontargeting negative control (5′-AAAUGUGAGAUCAGAGUAAU-3′) were used. Twelve thousand cells were seeded in a well of a 96-well plate. The following day, cells were transfected with Cas-9 sgRNA complex at a ratio of 250 ng/1.5pmol per protein using lipofectamine Cas9 plus (Invitrogen) and lipofectamine CRISPRMAX

(Invitrogen) reagents. Forty-eight hours posttransfection, the cells were diluted and seeded as one cell/well in 96-well plates. The cells were grown till confluence, and the CRISPR knockout was confirmed by immunoblotting using an anti-HSC70 antibody or anti-ARL5B antibody.

Purification of Golgi

Cells were grown to confluency in 150 mm dishes, and the Golgi was extracted using sucrose gradient centrifugation (62, 63). Briefly, the cells were homogenized by passing through a 25-gauge syringe. The homogenate was mixed with 62% sucrose and then overlaid with 4.5 ml 35% sucrose and 3.5 ml 29% sucrose. The gradient was centrifuged at 2, 85,000*g* for 2 h at 4 °C in a SW40Ti rotor (Beckman). The Golgi fractions were taken from 29 to 35% sucrose interface and confirmed by immunoblotting using anti-GM130 and anti-Stx6 antibodies.

Preparation of cytosol from HeLa cells

HeLa cells were grown to confluency in 100 mm dishes. The cells were homogenized by passing through a 25-gauge needle, and the homogenate was centrifuged at 80,000 r.p.m for 30 min at 4 °C (64). The supernatant was aliquoted and frozen.

In vitro *myristoylation of ARL5B*

In total, 100 μM of His-ARL5B was incubated with 140 μM of myristoyl CoA (Sigma Aldrich, M4414) and 1.2 μM of purified recombinant human NMT1 at 25 °C for 5 h (37). After precipitation with 35% ammonium sulfate, the myristoylated proteins were recovered by centrifugation at 10,000*g* for 15 min at 4 °C and resuspended in a buffer containing 50 mM Tris pH 8.0, 100 mM NaCl, 2 mM $MgCl_2$, and 2 mM DTT. The samples before and after myristoylation were resolved on a 10% Tricine-SDS PAGE (42) as well as a 15% tris-glycine SDS PAGE.

Fluorescence assay for nucleotide binding

The fluorescence measurements were performed at 30 °C in fluoromax-4 spectrofluorometer (Horiba). In total, 400 nM mantGDP/mantGMPPNP (Life Technologies) was added to the binding buffer containing 25 mM HEPES pH 7.5, 100 mM NaCl, 1 mM EDTA, 0.5 mM $MgCl_2$, 3 mM DMPC, and 0.1% sodium cholate. Once the fluorescence (λexcitation—352 nm and λemission—440 nm) was stabilized, 2 μM His ARL5B was added and the fluorescence was followed.

In vitro *reconstitution*

In total, 1 μM myr-ARL5B-GDP/myr-ARL5B-GTP was incubated with 15 μg Golgi membrane, 15 μg cytosol, in a buffer containing 50 mM Tris pH8.0, 25 mM KCl, 2 mM $MgCl_2$, 2 mM DTT, 5 mM ADP, and 1 mM GDP/GTP. The reaction was carried out at 37 °C for 30 min with gentle shaking in the presence and absence of HSC70 (0.5 μM). The binding reaction was stopped by incubating the reaction mix at 4 °C for 5 min. Further, the reaction was centrifuged at 19,000*g* for 5 min at 4 °C to separate the pellet and supernatant. The pellet was washed multiple times with the buffer containing 50 mM Tris pH8.0, 25 mM KCl, 2 mM $MgCl_2$, and 2 mM DTT. The binding of myr-ARL5B-GDP/myr-ARL5B-GTP with Golgi membrane was detected by immunoblotting using an anti-His antibody. The band density was quantified using ImageJ.

Statistical analysis

The statistical significance was determined using an unpaired two-tailed Student's *t* test or one-way ANOVA in GraphPad Prism software version 6.0. The data is represented as mean ± SEM. The significance is as follows: $p > 0.05$- ns (non-significant); $p \leq 0.05$ - *; $p \leq 0.01$ - **; $p \leq 0.001$ - ***, $p \leq 0.0001$ - ****.

Data availability

All the relevant data are within the manuscript and its Supporting information files. The raw mass spectrometry data and the annotated spectra have been deposited to "figshare" (https://doi.org/10.6084/m9.figshare.16429140.v2) as an online resource. The Mascot search results for PMF-based identification of HSC70 are provided in the supporting information (Table S1).

Supporting information—This article contains supporting information.

Acknowledgments—We thank Dr Subba Rao Gangi Setty (Indian Institute of Science, Bangalore), Dr Chandan Sahi (IISER Bhopal), and Fiona Houghton (The University of Melbourne) for helpful discussions. We acknowledge the Central Instrumentation Facility at IISER Bhopal and its personnel for access to mass spectrometry, ITC, and confocal microscopy facilities. We thank Dimple Pawar for helping in the MS data acquisition. We sincerely thank Dr R. Mahalakshmi and Altmash Khan for their assistance in CD data acquisition. We are grateful to Dr Varun Chaudhary (IISER Bhopal) for sharing the GAPDH antibody. We thank Professor Sean Munro (MRC Laboratory of Molecular Biology) and Professor Paul Gleeson (The University of Melbourne) for sharing the ARL5B constructs for mammalian expression. We acknowledge Sameena Parveen (IISER Bhopal) for suggestions in the manuscript. We also thank Rabiya Naaz for lab management.

Author contributions—E. J. and S. D. conceptualization; D. G. data curation; E. J., A. T., A. K., and D. G. formal analysis; E. J. and S. D. funding acquisition; E. J., A. T., A. K., D. G., J. S., and S. D. investigation; E. J., A. T., and D. G. methodology; S. D. project administration; E. J. and S. D. resources; E. J. and S. D. supervision; E. J., A. T., and D. G. validation; E. J., A. T., A. K., D. G., and J. S. visualization; E. J., A. K., and D. G. writing–original draft; E. J. and S. D. writing–review and editing.

Funding and additional information—This work was funded by the Department of Science & Technology (CRG/2019/004580) and IISER Bhopal. E. J. was supported with the DST-INSPIRE fellowship.

Conflict of interest—The authors declare that they have no conflicts of interest with the contents of this article.

Abbreviations—The abbreviations used are: ARL, ARF-like protein; CD, circular dichroism; CIMPR, cation independent mannose-6-phosphate receptor; GAP, GTPase-activating protein; GBP, GFP-binding protein; GDI, GDP-dissociation inhibitor; GEF, guanine nucleotide exchange factor; HSC70, heat shock cognate protein; ITC, isothermal titration calorimetry; MS, mass spectrometry; NBD, nucleotide-binding domain; PMF, peptide mass fingerprinting; SBD, substrate-binding domain.

References

1. Yu, C. J., and Lee, F. J. S. (2017) Multiple activities of Arl1 GTPase in the trans-Golgi network. *J. Cell Sci.* **130**, 1691–1699
2. Francis, J. W., Newman, L. E., Cunningham, L. A., and Kahn, R. A. (2017) A trimer consisting of the tubulin-specific chaperone D (TBCD), regulatory GTPase ARL2, and β-tubulin is required for maintaining the microtubule network. *J. Biol. Chem.* **292**, 4336–4349
3. Khatter, D., Sindhwani, A., and Sharma, M. (2015) Arf-like GTPase Arl8: Moving from the periphery to the center of lysosomal biology. *Cell. Logist.* **5**, e1086501
4. Pasqualato, S., Renault, L., and Cherfils, J. (2002) Arf, Arl, Arp and sar proteins: A family of GTP-binding proteins with a structural device for "front-back" communication. *EMBO Rep.* **3**, 1035–1041
5. Antonny, B., Beraud-dufour, S., Chardin, P., and Chabre, M. (1997) N-Terminal hydrophobic residues of the G-protein ADP-ribosylation factor-1 insert into membrane phospholipids upon GDP to GTP exchange. *Biochemistry* **36**, 4675–4684
6. Randazzo, P. A., Terui, T., Sturch, S., Fales, H. M., Ferrige, A. G., and Kahn, R. A. (1995) The myristoylated amino terminus of ADP-ribosylation factor 1 is a phospholipid- and GTP-sensitive switch. *J. Biol. Chem.* **270**, 14809–14815
7. Liu, Y., Kahn, R. A., and Prestegard, J. H. (2009) Structure and membrane interaction of myristoylated ARF1. *Structure* **17**, 79–87
8. Seabra, M. C., and Wasmeier, C. (2004) Controlling the location and activation of Rab GTPases. *Curr. Opin. Cell Biol.* **16**, 451–457
9. Garcia-Mata, R., Boulter, E., and Burridge, K. (2011) The "invisible hand": Regulation of RHO GTPases by RHOGDIs. *Nat. Rev. Mol. Cell Biol.* **12**, 493–504
10. Berg, T. J., Gastonguay, A. J., Lorimer, E. L., Kuhnmuench, J. R., Li, R., Fields, A. P., and Williams, C. L. (2010) Splice variants of SmgGDS control small gtpase prenylation and membrane localization. *J. Biol. Chem.* **285**, 35255–35266
11. Chandra, A., Grecco, H. E., Pisupati, V., Perera, D., Cassidy, L., Skoulidis, F., Ismail, S. A., Hedberg, C., Hanzal-Bayer, M., Venkitaraman, A. R., Wittinghofer, A., and Bastiaens, P. I. H. (2012) The GDI-like solubilizing factor PDEδ sustains the spatial organization and signalling of Ras family proteins. *Nat. Cell Biol.* **14**, 148–158
12. Donaldson, J. G., and Jackson, C. L. (2011) ARF family G proteins and their regulators: Roles in membrane transport, development and disease. *Nat. Rev. Mol. Cell Biol.* **12**, 362–375
13. Houghton, F. J., Bellingham, S. A., Hill, A. F., Bourges, D., Ang, D. K. Y., Gemetzis, T., Gasnereau, I., and Gleeson, P. A. (2012) Arl5b is a Golgi-localised small G protein involved in the regulation of retrograde transport. *Exp. Cell Res.* **318**, 464–477
14. Rosa-Ferreira, C., Christis, C., Torres, I. L., and Munro, S. (2015) The small G protein Arl5 contributes to endosome-to-Golgi traffic by aiding the recruitment of the GARP complex to the Golgi. *Biol. Open.* **4**, 474–481
15. Toh, W. H., Tan, J. Z. A., Zulkefli, K. L., Houghton, F. J., and Gleeson, P. A. (2017) Amyloid precursor protein traffics from the Golgi directly to early endosomes in an Arl5b- and AP4-dependent pathway. *Traffic* **18**, 159–175
16. Xu, Y., Ye, S., Zhang, N., Zheng, S., Liu, H., Zhou, K., Wang, L., Cao, Y., Sun, P., and Wang, T. (2020) The FTO/miR-181b-3p/ARL5B signaling pathway regulates cell migration and invasion in breast cancer. *Cancer Commun.* **40**, 484–500
17. Ishida, M., and Bonifacino, J. S. (2019) ARFRP1 functions upstream of ARL1 and ARL5 to coordinate recruitment of distinct tethering factors to the trans-Golgi network. *J. Cell Biol.* **218**, 3681–3696
18. Shi, M., Chen, B., Mahajan, D., Boh, B. K., Zhou, Y., Dutta, B., Tie, H. C., Sze, S. K., Wu, G., and Lu, L. (2018) Amino acids stimulate the endosome-to-Golgi trafficking through ragulator and small GTPase Arl5. *Nat. Commun.* **9**, 4987
19. Stricher, F., Macri, C., Ruff, M., and Muller, S. (2013) HSPA8/HSC70 chaperone protein: Structure, function, and chemical targeting. *Autophagy* **9**, 1937–1954
20. Sousa, R., and Lafer, E. M. (2015) The role of molecular chaperones in clathrin mediated vesicular trafficking. *Front. Mol. Biosci.* **2**, 26
21. Agarraberes, F. A., and Dice, J. F. (2001) A molecular chaperone complex at the lysosomal membrane is required for protein translocation. *J. Cell Sci.* **114**, 2491–2499
22. Kaushik, S., and Cuervo, A. M. (2019) The coming of age of chaperone-mediated autophagy. *Nat. Rev. Mol. Cell Biol.* **19**, 365–381
23. Rothbauer, U., Zolghadr, K., Muyldermans, S., Schepers, A., Cardoso, M. C., and Leonhardt, H. (2008) A versatile nanotrap for biochemical and functional studies with fluorescent fusion proteins. *Mol. Cell. Proteomics* **7**, 282–289
24. Katoh, Y., Nozaki, S., Hartanto, D., Miyano, R., and Nakayama, K. (2015) Architectures of multisubunit complexes revealed by a visible immunoprecipitation assay using fluorescent fusion proteins. *J. Cell Sci.* **128**, 2351–2362
25. Greene, L. E., Zinner, R., Naficy, S., and Eisenberg, E. (1995) Effect of nucleotide on the binding of peptides to 70-kDa heat shock protein. *J. Biol. Chem.* **270**, 2967–2973
26. Fourie, A. M., Sambrook, J. F., and Gething, M. J. H. (1994) Common and divergent peptide binding specificities of hsp70 molecular chaperones. *J. Biol. Chem.* **269**, 30470–30478
27. Lee, C., Kim, H., and Bardwell, J. C. A. (2018) Electrostatic interactions are important for chaperone–client interaction *in vivo*. *Microbiology (Reading)* **164**, 992–997
28. Kaushik, S., and Cuervo, A. M. (2012) Chaperone-mediated autophagy: A unique way to enter the lysosome world. *Trends Cell Biol.* **22**, 407–417
29. Wen, Z., Shu, Y., Gao, C., Wang, X., Qi, G., Zhang, P., Li, M., Shi, J., and Tian, B. (2014) CDK5-mediated phosphorylation and autophagy of RKIP regulate neuronal death in Parkinson's disease. *Neurobiol. Aging* **35**, 2870–2880
30. Marquer, C., Tian, H., Yi, J., Bastien, J., Armi, C. D., Yang-klingler, Y., Zhou, B., Chan, R. B., and Di Paolo, G. (2016) Arf6 controls retromer traffic and intracellular cholesterol distribution *via* a phosphoinositide-based mechanism. *Nat. Commun.* **7**, 11919
31. Rink, J., Ghigo, E., Kalaidzidis, Y., and Zerial, M. (2005) Rab conversion as a mechanism of progression from early to late endosomes. *Cell* **122**, 735–749
32. Collinet, C., Stöter, M., Bradshaw, C. R., Samusik, N., Rink, J. C., Kenski, D., Habermann, B., Buchholz, F., Henschel, R., Mueller, M. S., Nagel, W. E., Fava, E., Kalaidzidis, Y., and Zerial, M. (2010) Systems survey of endocytosis by multiparametric image analysis. *Nature* **464**, 243–249
33. Capmany, A., Yoshimura, A., Kerdous, R., Caorsi, V., Lescure, A., Del Nery, E., Coudrier, E., Goud, B., and Schauer, K. (2019) MYO1C stabilizes actin and facilitates the arrival of transport carriers at the Golgi complex. *J. Cell Sci.* **132**, jcs225029
34. Brien, M. C. O., Flaherty, K. M., Mckay, D. B., and Chem, D. B. J. B. (1996) Lysine 71 of the chaperone protein Hsc70 is essential for ATP hydrolysis. *J. Biol. Chem.* **271**, 15874–15878
35. Kirchner, P., Bourdenx, M., Madrigal-Matute, J., Tiano, S., Diaz, A., Bartholdy, B. A., Will, B., and Cuervo, A. M. (2019) Proteome-wide analysis of chaperone-mediated autophagy targeting motifs. *PLoS Biol.* **17**, 1–27
36. Greener, T., Zhao, X., Nojima, H., Eisenberg, E., and Greene, L. E. (2000) Role of cyclin G-associated kinase in uncoating clathrin-coated vesicles from non-neuronal cells. *J. Biol. Chem.* **275**, 1365–1370

37. Padovani, D., Zeghouf, M., Traverso, J. A., Giglione, C., and Cherfils, J. (2013) High yield production of myristoylated Arf6 small GTPase by recombinant N-myristoyl transferase. *Small GTPases* **4**, 3–8
38. Franco, M., Chardin, P., Chabre, M., and Paris, S. (1996) Myristoylation-facilitated binding of the G protein ARF1GDP to membrane phospholipids is required for its activation by a soluble nucleotide exchange factor. *J. Biol. Chem.* **271**, 1573–1578
39. Franco, M., Chardin, P., Chabre, M., and Paris, S. (1995) Myristoylation of ADP-ribosylation factor 1 facilitates nucleotide exchange at physiological Mg2+ levels. *J. Biol. Chem.* **270**, 1337–1341
40. Lodge, J. K., Jackson-Machelski, E., Devadas, B., Zupec, M. E., Getman, D. P., Kishore, N., Freeman, S. K., McWherter, C. A., Sikorski, J. A., and Gordon, J. I. (1997) N-Myristoylation of Arf proteins in Candida albicans: An *in vivo* assay for evaluating antifungal inhibitors of myristoyl-CoA: Protein N-myristoyltransferase. *Microbiology* **143**, 357–366
41. Shirai, A., Matsuyama, A., Yashiroda, Y., Hashimoto, A., Kawamura, Y., Arai, R., Komatsu, Y., Horinouchi, S., and Yoshida, M. (2008) Global analysis of gel mobility of proteins and its use in target identification. *J. Biol. Chem.* **283**, 10745–10752
42. Schägger, H. (2006) Tricine-SDS-PAGE. *Nat. Protoc.* **1**, 16–22
43. Lundmark, R., Doherty, G. J., Vallis, Y., Peter, B. J., and McMahon, H. T. (2008) Arf family GTP loading is activated by, and generates, positive membrane curvature. *Biochem. J.* **414**, 189–194
44. Progida, C., and Bakke, O. (2016) Bidirectional traffic between the Golgi and the endosomes - machineries and regulation. *J. Cell Sci.* **129**, 3971–3982
45. Gulbranson, D. R., Davis, E. M., Demmitt, B. A., Ouyang, Y., Ye, Y., Yu, H., and Shen, J. (2017) RABIF/MSS4 is a Rab-stabilizing holdase chaperone required for GLUT4 exocytosis. *Proc. Natl. Acad. Sci. U. S. A.* **114**, E8224–E8233
46. Takahashi, T., Minami, S., Tsuchiya, Y., Tajima, K., Sakai, N., Suga, K., Hisanaga, S., Ohbayashi, N., Fukuda, M., and Kawahara, H. (2019) Cytoplasmic control of Rab family small GTP ases through BAG 6. *EMBO Rep.* **20**, 1–18
47. Rüdiger, S., Buchberger, A., and Bukau, B. (1997) Interaction of Hsp70 chaperones with substrates. *Nat. Struct. Biol.* **4**, 342–349
48. Yang, F., Li, T., Peng, Z., Liu, Y., and Guo, Y. (2020) The amphipathic helices of Arfrp1 and Arl14 are sufficient to determine subcellular localizations. *J. Biol. Chem.* **295**, 16643–16654
49. Lu, L., Horstmann, H., Ng, C., and Hong, W. (2001) Regulation of Golgi structure and function by ARF-like protein 1 (Arl1). *J. Cell Sci.* **114**, 4543–4555
50. Fukuzono, T., Pastuhov, S. I., Fukushima, O., Li, C., Hattori, A., Iemura, S. ichiro, Natsume, T., Shibuya, H., Hanafusa, H., Matsumoto, K., and Hisamoto, N. (2016) Chaperone complex BAG2-HSC70 regulates localization of Caenorhabditis elegans leucine-rich repeat kinase LRK-1 to the Golgi. *Genes Cells* **21**, 311–324
51. Clerico, E. M., Tilitsky, J. M., Meng, W., and Gierasch, L. M. (2015) How Hsp70 molecular machines interact with their substrates to mediate diverse physiological functions. *J. Mol. Biol.* **427**, 1575–1588
52. Kampinga, H. H., and Craig, E. A. (2010) The HSP70 chaperone machinery: J proteins as drivers of functional specificity. *Nat. Rev. Mol. Cell Biol.* **11**, 579–592
53. Craig, E. A., and Marszalek, J. (2017) How do J-proteins get Hsp70 to do so many different things? *Trends Biochem. Sci.* **42**, 355–368
54. Soldati, T., Riederer, M. A., and Pfeffer, S. R. (1993) Rab GDI: A solubilizing and recycling factor for rab9 protein. *Mol. Biol. Cell* **4**, 425–434
55. Dirac-Svejstrup, A. B., Soldati, T., Shapiro, A. D., and Pfeffer, S. R. (1994) Rab-GDI presents functional rab9 to the intracellular transport machinery and contributes selectivity to rab9 membrane recruitment. *J. Biol. Chem.* **269**, 15427–15430
56. Seow, T. K., Ong, S.-E., Liang, R. C. M. Y., Ren, E.-C., Chan, L., Ou, K., and Chung, M. C. M. (2000) Two-dimensional electrophoresis map of the human hepatocellular carcinoma cell line, HCC-M, and identification of the separated proteins by mass spectrometry. *Electrophoresis* **21**, 1787–1813
57. Sun, W., Xing, B., Sun, Y., Du, X., Lu, M., Hao, C., Lu, Z., Mi, W., Wu, S., Wei, H., Gao, X., Zhu, Y., Jiang, Y., Qian, X., and He, F. (2007) Proteome analysis of hepatocellular carcinoma by two-dimensional difference gel. *Mol. Cell. Proteomics* **6**, 1798–1808
58. Tamkun, J. W., Kahn, R. A., Kissinger, M., Brizuela, B. J., Rulka, C., Scott, M. P., and Kennison, J. A. (1991) The arflike gene encodes an essential GTP-binding protein in Drosophila. *Proc. Natl. Acad. Sci. U. S. A.* **88**, 3120–3124
59. Micsonai, A., Wien, F., Kernya, L., Lee, Y. H., Goto, Y., Réfrégiers, M., and Kardos, J. (2015) Accurate secondary structure prediction and fold recognition for circular dichroism spectroscopy. *Proc. Natl. Acad. Sci. U. S. A.* **112**, E3095–E3103
60. Micsonai, A., Wien, F., Bulyáki, É., Kun, J., Moussong, É., Lee, Y. H., Goto, Y., Réfrégiers, M., and Kardos, J. (2018) BeStSel: A web server for accurate protein secondary structure prediction and fold recognition from the circular dichroism spectra. *Nucleic Acids Res.* **46**, W315–W322
61. Costes, S. V., Daelemans, D., Cho, E. H., Dobbin, Z., Pavlakis, G., and Lockett, S. (2004) Automatic and quantitative measurement of protein-protein colocalization in live cells. *Biophys. J.* **86**, 3993–4003
62. Galen, J. van, and Blume, J. von (2013) Enrichment of Golgi membranes from HeLa cells by sucrose gradient ultracentrifugation. *Bio Protoc.* **3**, e906
63. Blume, J. Von, Alleaume, A. M., Kienzle, C., Carreras-Sureda, A., Valverde, M., and Malhotra, V. (2012) Cab45 is required for Ca2+;-dependent secretory cargo sorting at the trans-Golgi network. *J. Cell Biol.* **199**, 1057–1066
64. Aepfelbacher, M., Trasak, C., Wilharm, G., Wiedemann, A., Trülzsch, K., Krauss, K., Gierschik, P., and Heesemann, J. (2003) Characterization of YopT effects on Rho GTPases in Yersinia enterocolitica-infected cells. *J. Biol. Chem.* **278**, 33217–33223